Electrochemical Studies of Biosensor Mediators

By

Margaret Caroline Calhoun

Dissertation

Submitted to the Faculty of the

Graduate School of Vanderbilt University

in partial fulfillment of the requirements

for the degree of

DOCTOR OF PHILOSOPHY

in

Chemistry

May 13th, 2022

Nashville, Tennessee

Approved:

David E. Cliffel, Ph.D.

Lauren E. Buchanan, Ph.D.

Janet E. Macdonald, Ph.D.

Nathan D. Schley, Ph.D.

Jonathan G. Schoenecker, M.D., Ph.D.

For my mother, Teri.

She was unable to live her dream, so I live mine.

ACKNOWLEDGEMENTS

I would first like to thank Vanderbilt University and the Chemistry Department for providing me with the opportunity and resources to study at this institution. I would like to thank the funding sources over the past few years. My research would not have been possible: the U. S. Environmental Protection Agency (EPA 83950101) and the National Institute of Health (NIH R01 HD102752).

Thank you to past Cliffel Lab members Dr. Evan Gizzie, Dr. David "Dave" Crisostomo, Dr. Adam Travis, Dr. Dilek Dervishogullari, Dr. Ethan McClain, and Dr. Sara Melow. Thank you to the current Cliffel lab group: Kaixuan "Kysha" Xu, Grace Buckey, Nicholas Hortance, William Lowery, Olivia Owens, Pragun Tuladhar, Samantha Calvez, Matt Galazzo, and LTC John Williams II. They never fail to make me laugh when I show up, which is usually what I need.

Thank you to my committee: Dr. Lauren Buchanan, Dr. Janet Macdonald, Dr. Nathan Schley, and Dr. Jon Schoenecker. They have been endlessly patient, and I am forever grateful for it. I couldn't ask for a better committee, gracious but challenging.

My PI, Dr. Cliffel, has been one of the most gracious and generous men I have known. He has taught me often to give others the benefit of the doubt and has helped me harness my "enthusiasm" into a politically worded email, a skill I will take with me forever. I always knew he would make me a better electrochemist but being more political so as not to give myself more gray hair; I might value that skill more. No one tell him.

Former Cliffel Lab members Dr. Kody Wolfe and Dr. Chris Stachurski helped me with experiments, analyzed data, and road-tripped with me to a conference. Both have helped me at my lowest, and I wouldn't be here at the finish line without you guys.

I need to acknowledge those still in my life after a long time. Thank you to Scott Harding and Sunshine Morgan. To have some of my high school teachers still in touch with me and invested in my journey after all this time is an honor. Sunshine helped remind me every day that challenging moments are temporary, a skill that works well for life in general but amazing in graduate school. Scott used to tell my class, “It’s better to be bold and wrong than to be meek and right.”, so everyone now knows why I asked so many questions in classes.

Andrea Franco and I became friends during our first gen. chem lab in our first semester of undergrad, and we are still friends now. While our dreams of being forensic scientists changed, our friendship hasn’t. Time and distance haven’t changed anything, and someday we will be able to get doughnuts and macarons together again.

I want to thank Peg Leonard-Martin, Brian Pollack, Jennifer Smith, and Stacey Satchell for helping me learn the coping skills I needed to finish my Ph.D. and become a healthier human being overall. It’s easy to put in the work to get better when you know the people working with you are skilled individuals and believe in you.

Thank you to Dr. Aaron Daniel. I have told him before words are beyond how thankful I am to have him in my life. There are not many people you can run into their office and say, “I have a math emergency!” and they will be able to help you. He edits everything I write and whatever hits Dr. Cliffel’s desk is usually coherent because of him. He’s a fantastic friend, always has my back, and more importantly, he calls me out when I’m wrong. Thank you for being one of my dearest friends.

Finally, thank you to my family, Andre, Nancy, Grandpa, and Grandma, for being interested, even if you weren’t sure what was going on. And thank you for also knowing when I’d rather not talk about it. A tightrope I appreciate you walking for me.

Mom, Dad, and Amelia: Thank you for supporting me through this. I could go on forever about it (absolutely rambling), but this is best kept simple. You always knew I could, and reminded me I could, every time I thought I couldn't. You have all contributed to this dissertation; it's as much yours as mine. I love you all.

Table of Contents

List of Figures

List of Tables

1. INTRODUCTION

Electrochemistry is a branch of science that has permeated our society more than one might expect. The 2019 Nobel Prize in chemistry was awarded for the development of Li-ion batteries, an item that has made its way into a variety of electronic devices.[1] Electrolysis is used for thin film creation and electroplating, coatings necessary for long-term preservation of aircraft and ships, and provides creative applications for artists and craftspeople.[2-4] Scanning electrochemical microscopy and its offshoots have just passed the 30-year mark of surface characterization.[5] Spectro-electrochemistry is an area that couples electrochemistry with one of the varieties of light analysis methods available (IR, lasing analysis, UV-vis, and fluorescence, to name a few).[6] Photo-electrochemistry and photovoltaics look at the creation and study of solar cells through their electrochemistry.[7] Small profile and high sensitivity electrodes have made a popular platform to build biosensors.[8-9] One of the more recent fields to arise is electrochemistry, and the potentiostat as the mechanism for oxidation or reduction in synthetic reactions, removing the harsh chemicals often required previously.[10]

Within many of these listed applications is the electrochemical mediator. An electrochemical mediator is an electrochemically active compound used to move electrons around within a system in a charge or electron transfer capacity.[11] Electrochemical or redox mediators are required for various electrochemical applications. While the exact function of an electrochemical mediator will change depending upon the application, several characteristics are agreed upon across the multiple uses that create a standard definition. In the 1980s, Fultz and Durst worked to develop a well-rounded description of a bio-redox mediator.[12] the ideal characteristics for vetting new mediators for such systems were compiled from an exhaustive literature search. While these

are based explicitly around biological systems, their tenets appear to hold for mediators in other applications as well:

1) well-defined electron stoichiometry

2) known formal potential

3) fast heterogeneous and homogeneous electron transfer

4) ready solubility in aqueous media at or near pH 7

5) stability in both oxidized and reduced forms

6) no optical interference where optical monitoring of the biological compound is used

7) no interaction with the biological compound in a manner that alters its redox potential

1) well-defined electron stoichiometry

This idea looks at the mediator redox couple mechanism. Redox reactions, like chemical reactions, are written out and balanced with proper stoichiometry. In the case of redox reactions, since electrons are a crucial part of the electrochemistry, the electrons are included in the reactions and must also be balanced. Specific redox reactions might not require many side reactions for the electrons to transfer. The reaction might be one where the reaction conditions affect the number of electrons that transfer (pH, temperature, catalyst). The stoichiometric transfer of electrons should be easy to deduce from experimentation and agreed upon in the literature.

2) known $E_{1/2}$ potential

The $E_{1/2}$ potential is the potential of a half-cell (half-reaction) measured against the standard hydrogen electrode.[6] Like the electron-stoichiometry above, this potential should be consistent during experimentation and agreed upon by the literature.

3) fast heterogeneous and homogeneous electron transfer

When electrochemists discuss the 'kinetics' of an electrochemical reaction, they discuss the number of steps required to complete the redox reaction (chemical and electron transfer) and the slowest step's kinetics.[6] Additionally, homogenous electrochemical redox occurs when electron transfer occurs between two chemical species. In contrast, heterogeneous redox is where the electron transfer occurs between a chemical species and the electrode surface. The speed of the mediated electron transfer should be fast whether it occurs with other chemical species or at the electrode surface.

4) ready solubility in required media and pH (adapted)

Adapted for all situations, meditator molecules must be able to move quickly around their environment. A highly soluble mediator (in the application solvent) will allow it to diffuse rapidly in its environment, improving electrochemical kinetics and charge transfer.

5) stability in both oxidized and reduced forms

Since the mediator's purpose is to transfer electrons within its application, it will contain more electrons at specific time points (in its reduced form) and contain fewer electrons at other time points (in its oxidized form). If the mediator compound is chemically unstable in either the oxidized or reduced forms, it will be unlikely to stay at the desired concentration or accept or donate the electrons. Additionally, unstable compounds within the mediator's application might cause additional problems such as unwanted byproducts or the degradation of other materials.

6) no measurement interference for characterization purposes (adapted)

Mediators are often a background means of accomplishing another chemical goal. If they interfere or drown out the desired signals that are looking to be measured with required characterization methods, then the mediator is not being "benign" as needed.

7) no interaction with the system in a manner that alters its redox potential

As with parameter 6, a mediator might be "benign" in its intended application, and a shift in redox potential would be a severe effect. While not affecting the redox potential is one hurdle, testing three mediators within a system and using them in all forms of characterization, if possible, would arguably be the best method of determining which mediator has the smallest effect on the system.

Uses

A brief literature review found mediator electrochemistry to fall into four categories: fuel and photovoltaic cells, microbial fuel cells, biosensors, and protein sensors. Mediators are required for fuel/photovoltaic cells to assist in the alignment of the thermodynamics, kinetics, and bandgaps within them to help the electrons or excitons (bound state of an electron and electron-hole which are attracted to each other by electrostatic Coulomb force) to move across them.[13-14] Microbial fuel cells are made to produce a fuel or for bioremediation, and the bacteria within them release a variety of mediators, therefore requiring study.[15-16] Enzyme biosensor design has evolved into two generations, I and II, where generation I placed an enzyme over the top of the electrode and the turnover of the enzyme when in the presence of its substrate produced hydrogen peroxide, a mediator that was used by the electrode to detect the presence of the substrate.[17] To improve this design, generation II moved towards redox polymer mediators. These thin films could transfer the electrons towards the electrode surface via the metal centers on the polymers with the enzyme held within.[17] For protein detection, mediators are usually required due to either adsorption on the electrode surface that leads to an inconsistent signal, or the proteins metal center(s) do not provide a signal to be detected, and a mediator is used to enhance the signal.[18]

Advantages and Drawbacks

The advantage of using a mediator is their primary function, assisting in charge transfer within a system. Their mobility and reversibility allow them to perform redox that the systems they are deployed in cannot, allowing the chemistry to occur there when it otherwise would not. Additionally, with many available mediators, there comes a wide range of customizability. This is an extreme advantage when aligning a bandgap for fuel or photovoltaic cells. Sometimes more than one mediator can be used to help with this issue.[19] Biosensors also benefit from this advantage since mediators might react poorly with a given biological compound or within a matrix but work well with another.

There are several drawbacks to mediators. The first is that while their electrochemistry is predictable, they add an additional variable to the system of study, and it can interrupt any alternative measurements if you are not in control of the mediator concentration. With the study of certain bacteria for microbial fuel cells for energy or environmental remediation, there are several proposed possibilities to which avenue of their deployment is most effective, some direct, some mediated. However, the bacteria are secreting and excreting the mediators. This makes it extremely difficult, if not impossible, with the current instrumentation to study the extracellular electron transfer.[15-16] Another concern with mediators is if they perform unwanted chemistry with the surrounding environment. While it is stated that a good mediator does not interact with the biological compound in a manner that alters its redox potential, the mediator reacting with other portions of the system can also cause issues. Since the electrode is the sensor, adsorption or polymerization is an issue that can dampen the signal. This is a concept that will be further explored in this work.

2. ELECTROCHEMICAL METHODS

Chapter 2 contains a general description of the instrumentation used throughout the research discussed in this dissertation. The application of specific protocols can be found in the corresponding chapters.

2.1. Standard Electrochemical Cell

This dissertation will rely on the standard “3-electrode cell" for electrochemical experimentation shown in Figure 2.1.

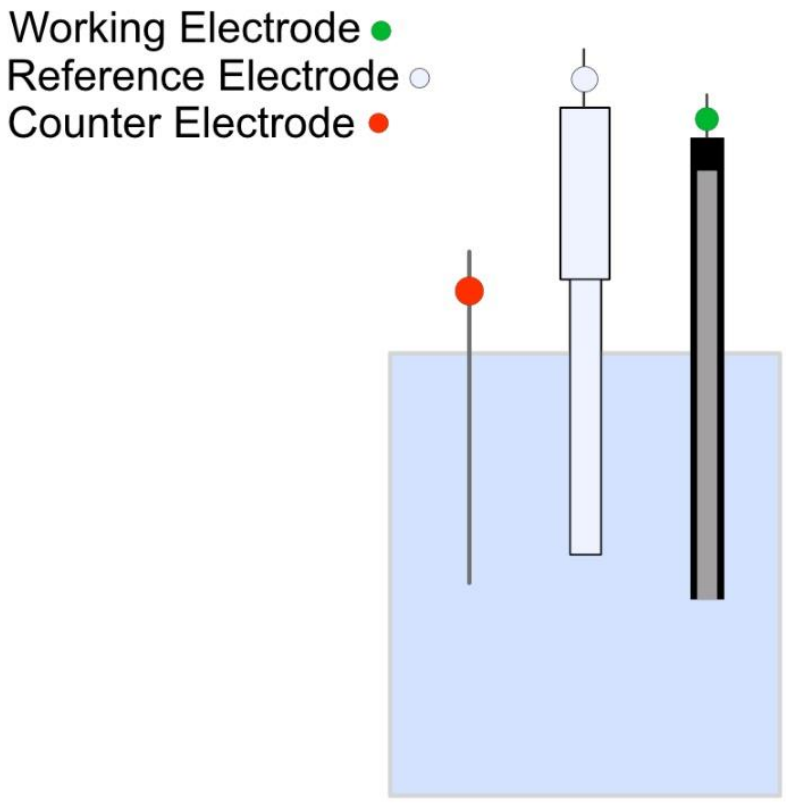

Figure 2.1. Standard 3-electrode cell. The three-electrode cell consists of an electrolyte solution, a working electrode (green), a reference electrode (white), and a counter electrode (red).

This involves a container full of aqueous solution with a solubilized ionic conductor or electrolyte. This solution can contain other solutes, often ones deemed for characterization. Inside this solution, three electrodes will be submerged: a working electrode (when applicable denoted as green), a reference electrode (white), and a counter electrode (red). The working electrode is where a change in the system is induced, and measurements are taken. This is also the electrode where films are applied for study or sensors are attached. The reference electrode (Ag/AgCl for this work) is used as a standard to allow electrochemists to study one-half reaction at a time. Reference electrodes are made of highly stable reactions and therefore do not shift around due conditions. This allows for their packaging into neat electrodes for use repeatedly in multiple experiments and gives a standard for comparison. The counter electrode provides a low-impedance path for current to flow through during experimentation. While a two-electrode system using the working and reference electrodes could perform this task, the noise and potential offset during an experiment are lower when a counter electrode is used. Pt wire or mesh is often used as the counter electrode. Screen-printed electrode (SPE) production will often use the ink used on the working electrode for the counter electrode to minimize the steps in the manufacturing process.

2.2. Cyclic Voltammetry

A cyclic voltammogram (CV) is a voltammetric technique, meaning that the current response of a sample solution is recorded while a potential sweep is performed.

The power of the CV as a characterization method comes from its waveform and the potential applied vs. time throughout the experiment (Figure 2.2).[20]

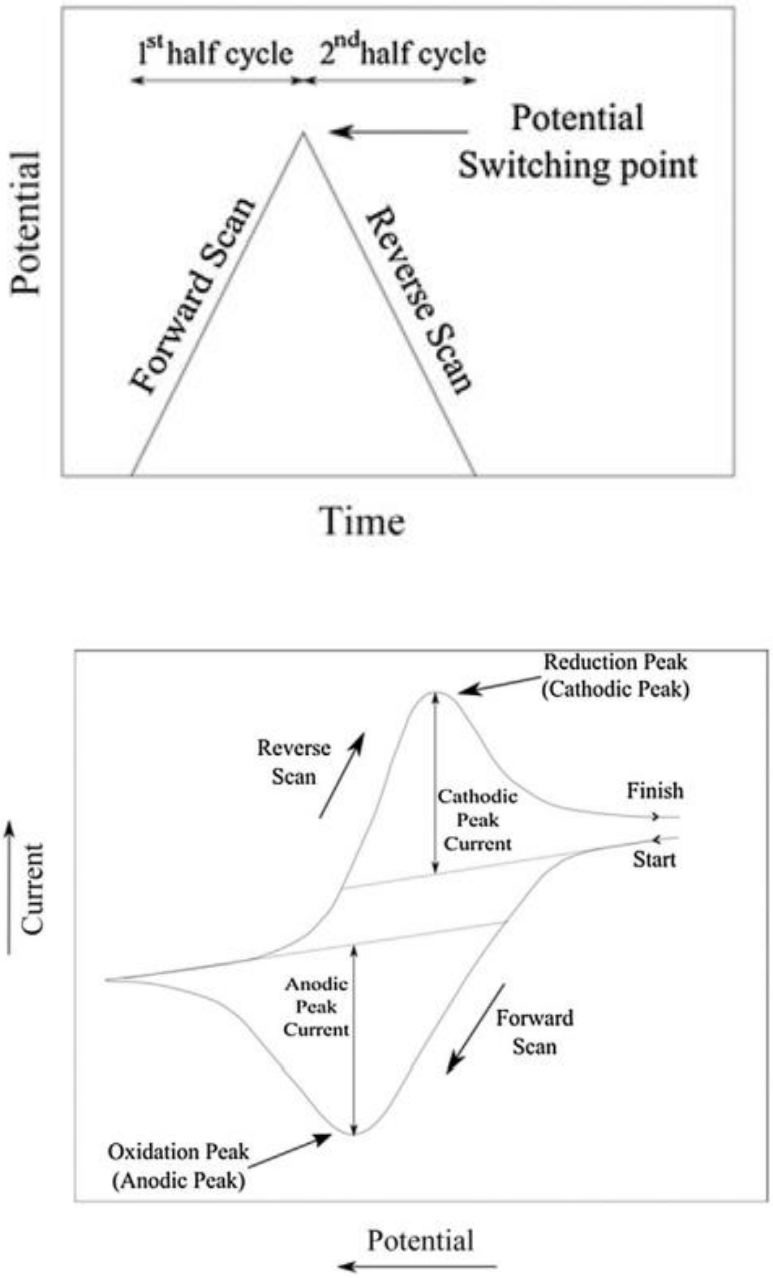

Figure 2.2. Cyclic Voltammetry Waveform and example CV. The top shows the waveform of a CV, the potential vs. time during the experiment. The bottom shows an example cyclic voltammogram with parts labeled.

For the CV, the potential moves at a single scan rate, υ, to the switching potential, λ, and then scanning back to the starting potential. This cycle forms the signature "duck" shape, as shown in Figure 2.2.

The peaks obtained in a CV show the reduction and oxidation potentials of the substance in the experiment. The ratio of the peak heights assesses the electrochemical reversibility of the substance. A compound can be reversible, irreversible, or quasi-reversible, and the ratio of the peak heights determines which category it falls into. Completely reversible compounds have nearly equivalent peaks, and this means that the compound freely cycles between its oxidized and reduced forms (ex: the ferri/ferrocyanide couple). Irreversible couples will only redox one direction and will be missing a redox peak during their CVs. This is due to a chemical or morphological change that makes the substance electrochemically inactive once it has gone through its first half of the CV (ex: Vitamin C). Quasi-reversible couples have uneven redox peaks, meaning that one half of the redox reaction is easily oxidized or reduced, and the other half is still electrochemically available to engage with the electrode; however, its electron transfer is slow, either due to kinetics or thermodynamics (see below). This means a lower current flow during this half of the redox and thus a smaller peak. The difference between where the peak potentials occur also provides insight into the electrochemical behavior seen during a CV. If the behavior is reversible and "Nernstian" the difference between the two potentials where the peaks occurred (known as peak splitting) should be 59 mV/n, where n is the number of electrons transferred during the reaction. Deviation from this has implications in regards to the thermodynamic behavior of the system (less favorable is more than 59 mV).[6]

Like traditional chemical reactions, electrochemical reactions have thermodynamic and kinetic components. Crudely, thermodynamic behavior is seen in the potentials of reactions,

whereas the currents and peak heights are where kinetic behavior is seen. This is where the limitations of CV as a technique begin. Basic knowledge about the compound studied can be deduced (reversibility) and possibly what behavior to further investigate if needed (thermodynamically controlled behavior vs. kinetically controlled behavior). However, additional experiments and techniques will need to be employed to gain more information.

2.3. Square Wave Voltammetry

Square Wave Voltammetry (SWV) is a methodology where the current is measured while the potential is varied; however, the potential waveform is more complicated. In Figure 2.3, the waveform is shown for SWV and is known as a "staircase on a ramp". Due to its difficulty, it was not developed until computer-controlled potentiostats were widely available. This method allows for more sensitivity as this method lowers the noise. [20]

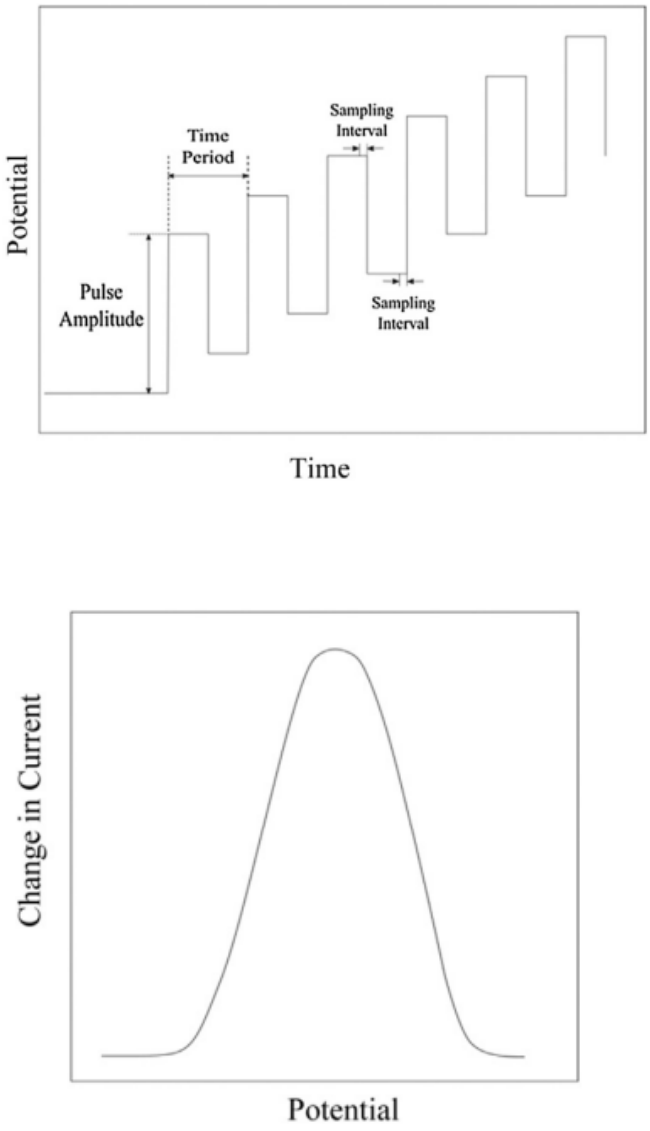

Figure 2.3. Square Wave Voltammetry Waveform and example SWV. The top shows the waveform of a SWV, the potential vs. time during the experiment. The bottom shows an example square wave voltammogram.

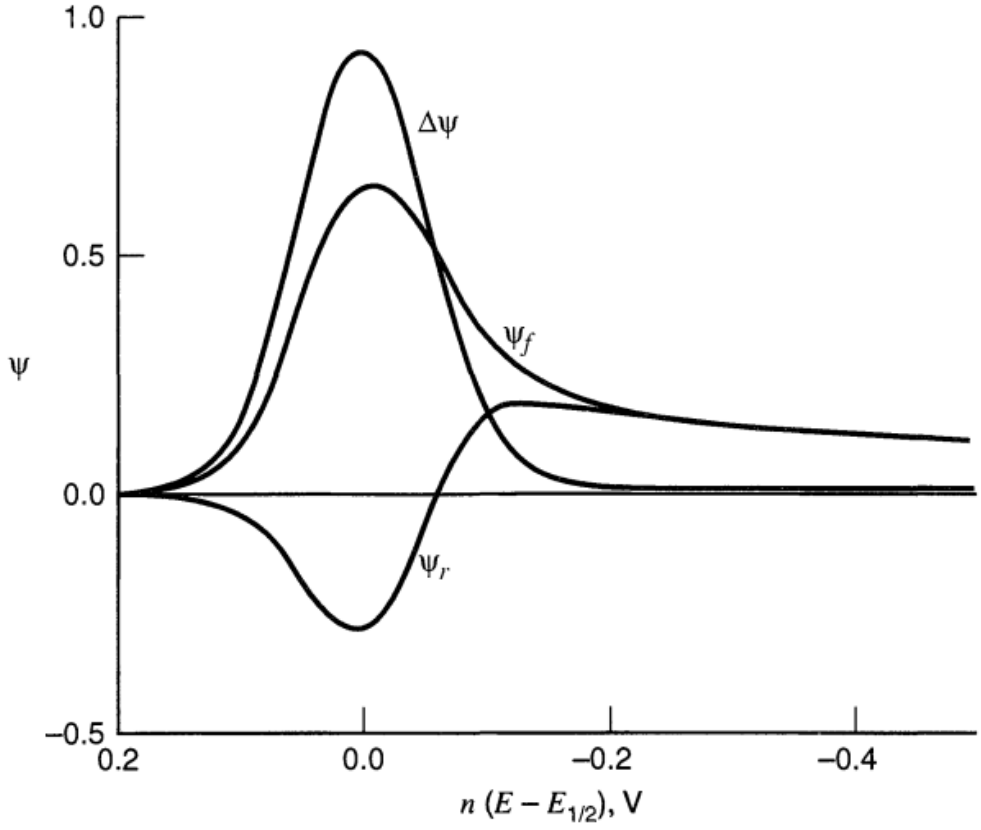

Figure 2.4. SWV Forward, Reverse, and Difference Scans. The scans overlaid demonstrate the amplification of signal that SWV can provide.

As shown above, in Figure 2.4, the forward and backward reaction combinations amplify the peak signal.[6, 21] Systems with more complicated electrochemical kinetics will show this in the forward and reverse scans, as will more complex thermodynamic systems.

SWV is limited by its analysis of only one-half reaction of the redox couple studied. This requires recorded data from this technique to have an additional context or preliminary characterization. Therefore, SWV should be used as a follow-on technique. Additionally, while helpful in discovering subtle information, its sensitivity can result in vast experimentation and troubleshooting with parameters to get meaningful results.

2.4. Chronoamperometry or Amperometric i-t Curves

Amperometric methods differ from voltammetric methods by measuring current versus time while a potential hold is applied. This can be used for both characterization and sample detection purposes. Applying one potential and then looking at the resulting current decay should follow the Cottrell equation (equation 2.1). Note that the Cottrell equation only holds when the electrochemical kinetics are fast/instantaneous, and the electrode is macroscale in size. However, even if a system exhibits non-Cottrellian behavior, a calibration can still be made between current and concentration.[6]

$$i = \frac{nFAD^{1/2}C_o^*}{\pi^{1/2}t^{1/2}} \qquad \text{(Equation 2.1)}$$

In this equation, current (i) is equal to the number of electrons being transferred (n) times the area of the electrode (A), times the square root of diffusion of the molecule ($D^{1/2}$), times

Faraday's constant (F), times the initial concentration of the reactant (C_o^*). This is divided by $\pi^{1/2}$ times the square root of time ($t^{1/2}$). This equation is important due to the number of essential factors that it accounts for, such as diffusion and the number of electrons being transferred. However, what most focus on is that the initial concentration of analyte at the electrode surface is in this equation. This allows for the concentration of the analyte to be calculated if the analyte is of typical diffusion speed and the number of electrons in the redox process is known.

Since this method reports current vs. time, it is helpful in real-time measurement sensor development. Organ-on-a-chip and biosensor teams use this methodology to create calibration curves in flow cells and microfluidics.

Limitations to this technique come from the application of one potential. Previous experimentation and characterization need to have been performed before using this technique to determine the correct parameters for these experiments.

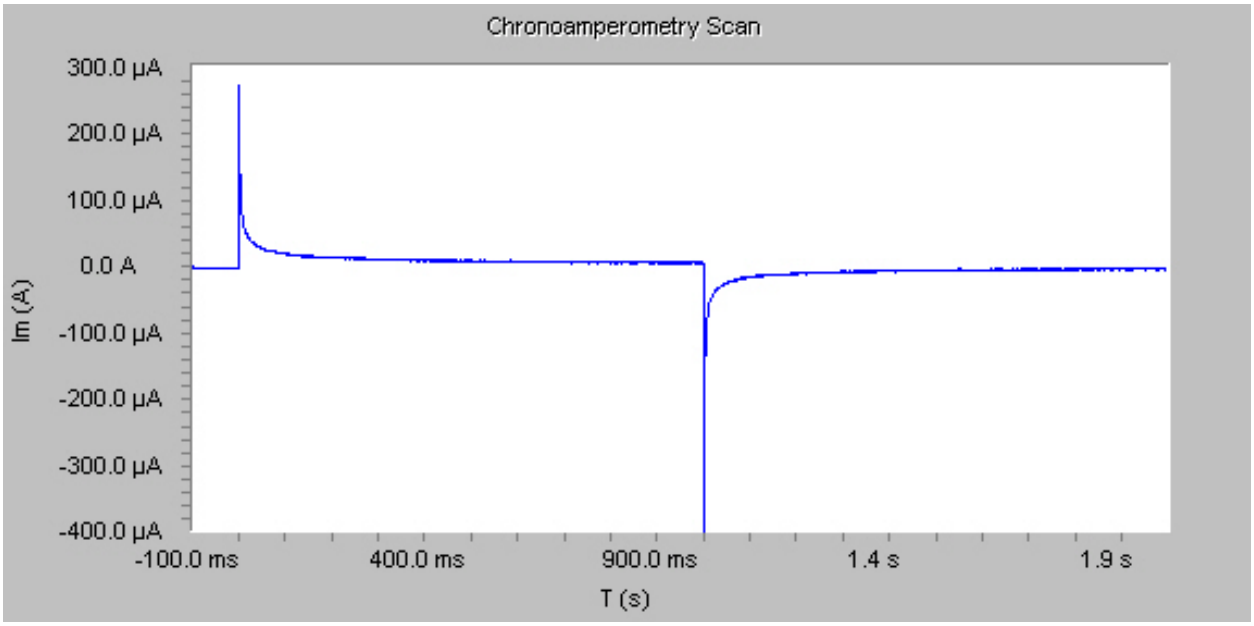

Figure 2.5. Chronoamperometry waveform and example scan. An example CA experiment.[22]

3. OSMIUM REDOX POLYMER MEDIATOR FOR WIRED ENZYMATIC BIOSENSORS

Chapter 3 shows the effects of trace oxygen upon the osmium precursor for a redox polymer commonly utilized within wired enzymatic biosensors. This research was assisted by Dr. Christopher Stachurski, Dr. Aaron Daniel, and Dr. Nathan Schley. They further assisted in the preparation of this manuscript.

3.1 TRACE OXYGEN AFFECTS OSMIUM REDOX POLYMER SYNTHESIS FOR WIRED ENZYMATIC BIOSENSORS,[23]

3.1.1. Introduction

Biosensors are commonly utilized throughout medical, environmental, and food safety applications.[17, 24] Enzyme-based electrodes are a leading platform for these uses. The electrochemical enzyme biosensor comprises an enzyme immobilized onto an electrode surface. When the substrate turns over at the enzyme, a redox cofactor is required to assist the enzyme in transforming the substrate. Since these redox co-factors must be recycled for another enzymatic reaction to occur, a mediator is typically used to recharge these co-factors.

Based on the electrochemical mediator used to recharge the enzymatic co-factor, the enzyme biosensor can be broadly classified as either Type I (oxygen mediated) or Type II (redox polymer mediated) (Figure 3.1). Both types of sensors are commercially, clinically, and in research today. In a Type, I biosensor, the electrons released by the enzyme-substrate turnover are accepted by a small molecule redox couple that diffuses to the underlying electrode. A common Type I example is oxidase enzyme electrodes, where oxygen naturally dissolved in water recharges the co-factors by accepting the electrons and becoming hydrogen peroxide. Hydrogen peroxide is collected by the underlying electrode set to a potential to oxidize the peroxide, producing a current.

Different amounts of a substrate can be exposed to the enzyme, producing different amounts of the corresponding current recorded to create a calibration curve. Once this has been established, an unknown substrate concentration can be detected. This concept is the original methodology for the modern blood glucose meter and is known as a "Type I" enzyme sensor, initially developed by Leland Clark (Figure 1, left) and launched an area of research that gave way to modern biosensors.[17]

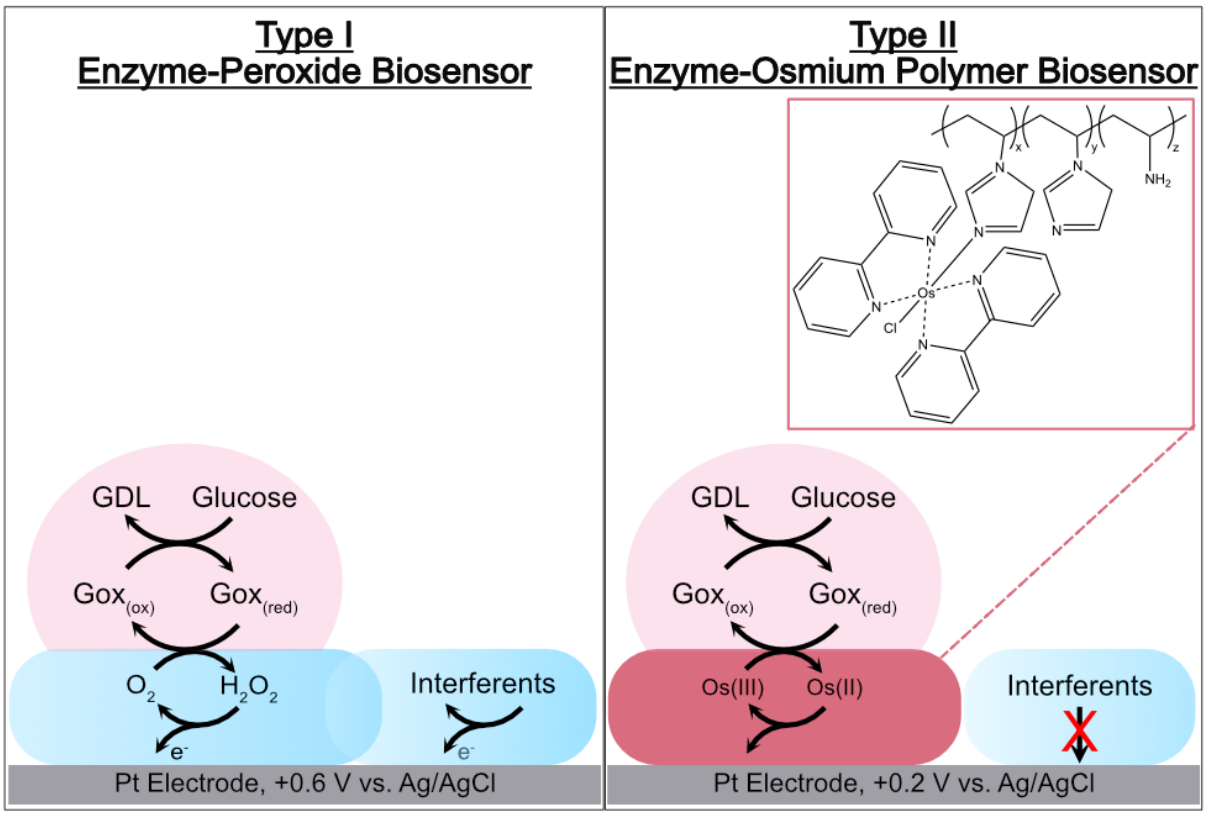

Figure 3.1. Type I vs. Type II Oxidase Enzyme Electrochemical Biosensors. In type I sensors, oxidase enzymes react with dissolved oxygen in solution to produce hydrogen peroxide that is oxidized at the underlying Pt electrode. Type II sensors bypass peroxide by using a redox polymer to accept the electrons from the enzyme.

Type I enzyme biosensors are easy to develop as they involve very few components (typically only enzyme and potentially a crosslinker). Still, they are more inclined to measurement instability and interference since their measurements depend on oxygen and hydrogen peroxide, both biologically active. Measurement instability leads to issues with replication and sensitivity. With oxygen and hydrogen peroxide both biologically active, their concentrations could fluctuate due to general biological function or disease. Because the foundation of the sensor's mechanism is built around the concentration of oxygen and hydrogen peroxide, readings could be falsely shifted due to these fluctuations, such as the sensor's inability to function at low concentrations of oxygen from cell consumption or inflated concentration readings from increased hydrogen peroxide. This variability leads to sensor insensitivity when creating a baseline calibration curve or taking biological sample measurements. Hydrogen peroxide is also toxic to cells, contaminating the results of online in-vitro or in-vivo experiments. Since the redox potential is non-selective in solution, any other solute that is redox-active at that potential will contribute to the signal, along with the hydrogen peroxide. The potential required to detect hydrogen peroxide is the cause of most interference. With the oxygen/hydrogen peroxide redox couple as the mediator, it is possible that a variety of biological interferents will be contributing to the signal.

To eliminate the need for the reactive hydrogen peroxide/oxygen redox couple, there is a growing interest in using organometallic polymers in biosensors for electron mediation. There are also a variety of biological interferents that are necessary to eliminate for accurate measurements. The high oxidation potential used for peroxide detection can lead to problems with interferents such as acetaminophen. Acetaminophen can be oxidized near the same potential of the hydrogen peroxide; therefore, if a person had taken acetaminophen and then measured their blood sugar

levels, the electrode would not only report on the amount of hydrogen peroxide present (e.g., glucose), but the acetaminophen as well.[25]

Redox polymers are polymers that can be reversibly reduced or oxidized. There are an increasing number of uses in fuel cells, photovoltaics, and biosensors.[24] The redox activity of these polymers can originate from several sources, including organic functional groups, side-chains, and the inclusion of a transition metal center. Incorporating redox polymers into electrochemical systems can be advantageous due to the immobilization of reactive enzymes or proteins, increased structural stability, and assisting in mediated electron transfer (MET).[24] Redox polymers' ability to assist in MET has allowed advancement in enzymatic biosensors. Heller and co-workers developed the "Type II" sensor (Figure 3.1B),[26] utilizing a redox polymer as electrochemical mediators rather than oxygen and hydrogen peroxide. Heller was the first to describe an osmium polymer used in a biosensor, now considered the most popular strategy for achieving effective electrical wiring of redox enzymes.[26] The redox-active component of these polymers has an $E_{1/2}$ that is lower than the oxidation potential of acetaminophen and therefore would not oxidize acetaminophen at the electrode in the same way as the Type I sensors.[26-27]

In Type II biosensors, the electron generated from the enzyme turnover is accepted by the redox-active polymer and used as a mediator to shuttle the electrons to the underlying electrode surface. The mechanism of the polymer mediation is to use the organometallic portions of the polymer as the redox shuttle by hopping from organometallic complexes tethered within the polymer to transfer the electron down to the electrode surface. This means that the polymer unit length in combination with the "hardness" of the crosslinker needs to be fine-tuned to maximize the signal detected. Type II sensors are more challenging to develop because synthesizing the organometallic polymer can be time-consuming and complicated. Optimizing the sensor film

requires the proper thickness, loading of redox couple onto a polymeric backbone, and stability lifetime. The stability variables come from the amount of redox polymer, the amount of enzyme, and the type of crosslinker used.

The redox polymer utilized for the Type II biosensors described in this work is osmium (II) bis(2,2'-bipyridine) chloride-poly(vinylimidazole-allylamine) ($Os(bpy)_2Cl$-PVIAA). This compound is a widely used redox polymer in the field of biosensors.[25-29] This literature includes the syntheses of the $Os(bpy)_2Cl$-PVIAA polymer using an $Os(bpy)_2Cl_2$ precursor to facilitate the loading of the redox couple onto the PVIAA backbone. Most previous literature commonly references the syntheses from Meyer *et al.* and Buckingham *et al*., which both use the same protocol.[26-31] These two references detail nitrogen gas purges to provide an oxygen-free environment during the intermediate synthesis rather than more rigorous methods, such as a vacuum gas manifold.[32] Unfortunately, this literature does not include NMR structural analysis or mass spectrometry of the intermediates but focuses on other characterization methods such as absorbance or $E_{1/2}$ values. Finklea *et al*.[33-34] include NMR for the Os compounds in their synthetic papers.

During our synthesis of this osmium redox polymer, we determined that the synthesis of the intermediate Os complex was very sensitive to the effects of trace oxygen. The result of trace oxygen exposure to this intermediate resulted in a redox polymer that was no longer useful for the desired type II oxidase biosensor as its redox potential shifted to more positive potentials. Careful consideration of using a vacuum gas manifold for the oxygen-free synthesis is important during the Os complex intermediate synthesis, even though the desired Os redox polymer is not particularly oxygen sensitive. Here, we provide detailed protocols for the oxygen-free synthesis of $Os(bpy)_2Cl_2$ and additional compounds required to create $Os(bpy)_2Cl$-PVIAA. Structural, optical,

and electrochemical characterizations are given for the desired compounds and the oxygen-containing intermediates, which agree with the reported literature values. Based on mass spectrometry, NMR, luminescence, and electrochemical data, we conclude that $OsO_2(bpy)_2$-PVI is the resulting redox polymer from the exposure to trace oxygen during the synthesis.

3.1.2. Materials and Methods

Materials

$OsCl_3 \cdot 3H_2O$ (99.95%) was purchased from Strem Chemicals. Dimethylformamide (DMF; 99.9%) and 200- proof ethanol was obtained from Fisher Scientific. ^1H NMR solvents $CDCl_3$, D_2O, and Acetone-d_6 (99.9%) were obtained from Cambridge Isotope Lab Inc. The following chemicals were obtained from Sigma Aldrich: $(NH_4)_2OsCl_6$ (99.99%), 2,2’-bipyridine (reagent plus ≥99%), ethylene glycol (99.9%), anhydrous diethyl ether (99.9%), hydrochloric acid (HCl; 37% w/v), 1‑vinylimidazole (≥99.9%), allylamine (AA, 98%), sodium dithionite (technical grade) and azobisisobutyronitrile (AIBN; 99%).

Preparation of $Os(bpy)_2Cl_2$

Various methods from the literature were used to synthesize the $Os(bpy)_2Cl_2$ precursor; brief descriptions are all found below with the amended first:

From Meyer *et al.*,[30] one (1) equivalent of $(NH_4)_2OsCl_6$ and two (2) equivalents of 2,2’-bipyridine were refluxed in ethylene glycol for 45 min under N_2. Once cooled, an equi-volume amount of saturated aqueous sodium dithionite solution was added to the reaction mixture to reduce all Os to the 2^+ oxidation state. The purple-black precipitate was washed with cold water to remove ionic products and large volumes of ether to remove organic products. The results and discussion show that oxygen is a more critical contaminant than previous studies assumed. This

synthetic method was performed using a vacuum manifold to minimize the risk of oxygen exposure.

From Finklea *et al.*[33-34], 500 mg of $(NH_4)_2OsCl_6$ were combined with 350 mg of 2,2'-bipyridine in 10 mL of deoxygenated DMF. The mixture was refluxed under a blanket of N_2 for an hour. Once the solution was cooled to room temperature, a solution of saturated sodium dithionite reduced any Os(III) to Os(II), and the mixture was cooled further in an ice bath, filtered, and dried under vacuum.

From Mamo *et al.*[35], an adaptation of a $Ru(bpy)_2Cl_2$ synthesis from Togano *et al.*[36], 0.5g of $OsCl_3 \cdot 3H_2O$ was dissolved in 15 mL of 200-proof ethanol and 10 mL DI water and was refluxed with continuous N_2 bubbling for 4 hours. To this solution, 0.7 g of 2,2'- bipyridine dissolved in 10 mL of 200-proof ethanol and 2 mL of conc. HCl was injected, and the mixture refluxed for an additional 30 minutes. Subsequently, the solution was cooled, the liquid evaporated, filtered, and dried under vacuum.

Preparation of PVIAA

To synthesize poly(vinylimidazole-allylamine), 1.04 mL of 1-vinylimidazole, 0.750 mL allylamine, and 12 mL of 200-proof ethanol were combined in a three-neck round bottom flask and purged with N_2 for 15 minutes while agitating. During the purging process, a solution of azobisisobutyronitrile (AIBN) was prepared from 65 mg of AIBN and 2 mL of 200-proof ethanol. The AIBN solution was added to the N_2-purged reaction flask via syringe. The reaction vessel was placed into a preheated 85°C oil bath. While not typically advised due to the degradation of the AIBN, a slightly better yield was found when the reaction solution was already slightly warm.[37]

Preparation of Organometallic-PVIAA

To synthesize the final polymer, $Os(bpy)_2Cl_2$ and PVIAA were combined in 200-proof ethanol (10–15 mL in a 100 mL round bottom flask) and gently heated using an oil bath to 85°C, stirring for 48 hours with a reflux condenser that was capped to limit ethanol evaporation. During this time, the $Os(bpy)_2Cl_2$ was loaded onto the PVIAA backbone under reflux, providing a 1:10 molar ratio Os to imidazole.[26-27] At the end of 48 hours, the reaction mixture was cooled, and the ethanol was slowly evaporated using gentle heating and a N_2-stream until a small volume remained. The remaining solution was diluted with DI water then centrifuged to remove any unreacted organometallic compounds. The water was then divided further among centrifuge tubes, diluted with more 200-proof ethanol, and prepped for lyophilization (see SI). The resulting solids could then be dialyzed for a more uniform size, and the same procedure followed of dissolving in water, diluting in ethanol, and lyophilizing. This procedure is the same for both organometallic-PVIAA compounds discussed in this paper and any previous iterations that were used for experimentation.

Lyophilization Procedure

Labconco Freezone 4.5 Plus and associated products were used to perform lyophilization on all samples for this project. Products were solvent exchanged or diluted into D.I. water. The solution was then placed inside centrifuge tubes with holes made in the caps with hypodermic needles. The solution was placed inside each tube to the corresponding freeze line limit. Each tube was then placed inside liquid nitrogen until completely frozen. Once frozen, the tubes were placed into the compatible glass jar and rubber cap with glass tube and then placed onto the lyophilizer. Vacuum was then slowly applied. The tubes were periodically observed every 2-8 hours, depending upon the amount of liquid that was being lyophilized. Once the product is finished, this process might be repeated if dialyzed.

Dialysis

Spectra/Por Biotech Cellulose Ester MWCO 10K dialysis membrane was used to perform dialysis. Several inches of the membrane were cut from the roll, and the end was clasped with a magnetic dialysis clip. The membrane was opened, the fluid poured in, and the top was held with a non-magnetic dialysis clip to where no air was inside the membrane, only fluid. The foam was rubber banded to the clasps to ensure flotation, and the membrane was placed into a 1000-2000 mL container of D.I. water on a stir plate, constantly stirring for 18-24 hours.

Instrumentation & Characterization

Unless otherwise stated, all analyses were performed at an analyte concentration of 1 mg/mL. ^{1}H NMR (400 MHz) was performed in CD_3CN for 2,2' – bipyridine, $CDCl_3$ for $Os(bpy)_2Cl_2$, and $CO(CD_3)_2$ for the f-Os precursor. Both osmium organometallic polymers were dissolved in D_2O for their ^{1}H NMR spectra. Mass spectrometry was performed using a Thermo Liquid Chromatography/Mass Spectrometer Orbitrap 2 with electrospray ionization (ESI) in positive mode (Mass Spectrometry Research Center, Vanderbilt University). Fluorescence measurements were performed using a Varian Cary Eclipse fluorescence spectrophotometer with the excitation and emission slit widths set at 5 nm. The scan rate was set to 600 nm per minute with a data interval of 1 nm. Absorption experiments were performed to determine best which excitation wavelengths were suitable. An excitation wavelength was selected to ensure maximum light absorption and maximize emission if it were to occur. This is shown and elaborated on in Results and Discussion. Electrochemical measurements were taken using a CH Instruments 620A potentiostat and screen-printed electrodes (SPEs) from Pine Research Instrumentation with a 2 mm OD carbon working electrode, a Ag/AgCl reference electrode, and a carbon counter electrode.

3.1.3. Results and Discussion

Initial attempts at the synthesis of $Os(bpy)_2Cl_2$ were made following the procedures of Meyer *et al.*, Mamo *et al.*, and Finklea *et al.*, which describe the use of a reflux condenser and N_2 purging.[30, 33-35] Under these conditions, an unexpected osmium compound was obtained as the major product. The synthesis that provided $Os(bpy)_2Cl_2$ was by Meyer *et al.* but was performed with a vacuum gas manifold to prevent any chance of oxygen contamination during synthesis.

We employed electrospray ionization mass spectrometry and NMR spectroscopy to identify the unexpected Os complex. The resulting $OsO_2(bpy)_2$-PVIAA, compared to $Os(bpy)_2Cl$-PVIAA, was easily identified by its bright luminescence and a significant shift in its oxidation potential seen in the cyclic voltammetry.

Mass Spectrometry

The ESI mass spectrum of the oxygen-containing $Os(bpy)_2$ intermediate complex is shown in figure 3.2. Both the parent peak at 534.07 m/z and subpeak 379.01 m/z have a unique descending isotope spacing in the preceding peaks. This is indicative of osmium's presence due to its isotopic abundance.

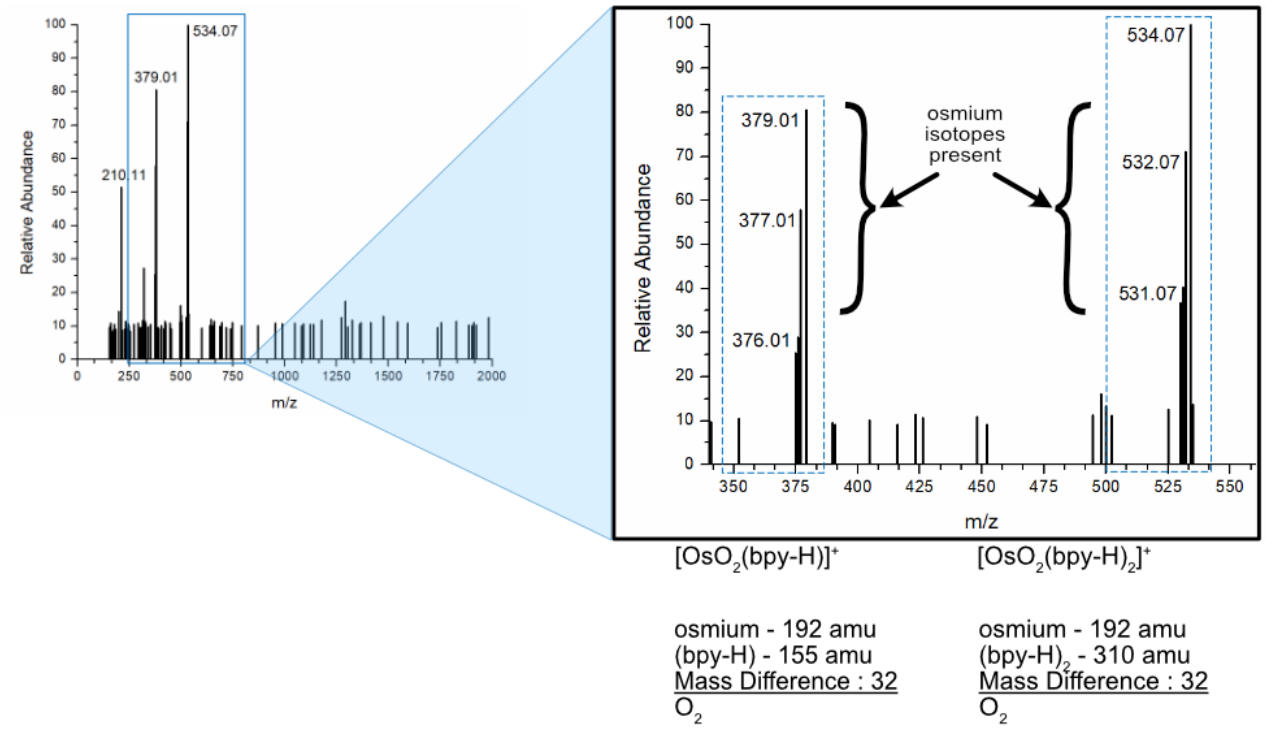

Figure 3.2. Mass Spectra of f-Os precursor or $OsO_2(bpy)_2$. The full spectrum is shown on the left, featuring the main peaks of the molecule and a zoom in on the right of the parent peak and subpeak at 534.07 and 379.01 m/z, respectively. The descending peaks indicate the osmium isotope's presence in each, and the significant weight to these compounds shows that bipyridine needs to be present in each molecule.

When further analyzing the two peaks, we see structural similarities. In the parent peak (534.07 m/z), once we account for the most abundant osmium-192 isotope (~40%), there is considerable mass left to the molecule. First, the base peak is assigned one osmium and two bipyridines based on the isotopic pattern. With that, we are left with a mass difference of 32 amu. In the subpeak (379.01 m/z), following the same process with one osmium-192 and a single bipyridine, we are left with a mass difference of 32 amu. Our results are consistent with a previous mass spectrometric analysis of unsaturated Os complexes with diatomic oxygen by Molina-Svendsen *et al.* In our data, the $OsO_2(bpy\text{-}H)^+$ was detected at 379 m/z from the addition of two oxygen atoms and with loss of the corresponding hydrogen from the now negatively charged bipyridine from the ESI process. For the base peak at 534.07 m/z, this mass to charge would suggest the $OsO_2(bpy\text{-}H)_2^+$ ion. Thus, we believe the identity of the organometallic that was consistently generated during the oxygen-contaminated synthesis of $Os(bpy)_2Cl_2$ is $OsO_2(bpy)_2Cl_2$ and $[OsO_2(bpy)]Cl_2$, which would then go on to form $OsO_2(bpy)_2$-PVI and $OsO_2(bpy)$-PVI. We will keep using the shorthand of f-Os-PVI for $OsO_2(bpy)_2$-PVIAA for the duration of this article, as we will use Os-PVI for $Os(bpy)_2$-PVIAA.

^{1}H NMR

Comparing the proton NMR spectra of the two polymers Os-PVI (figure 3.3, red, top) and f-Os-PVI (figure 3.3, blue, bottom), allows a direct comparison of their structural similarities and differences. Since these compounds are polymers, sharp peaks (e.g., ~8.4 ppm; ones expected in a typical small molecule NMR spectra) are contaminants that were not removed during attempts at purification. Peaks shown in the ~1.1-1.3 ppm range represent hydrogens on primary, secondary, and tertiary carbons in the backbone of the polymer chain. The broad peak at ~2-2.2 ppm also

represents the hydrogens in the backbone of the polymer chain. Since they are almost always in positions that are a carbon removed from aromatic groups, they behave as “benzylic”, explaining their ppm shift, higher relative signal, and broadening. The same scenario applying to vinylic hydrogens would explain the small, rounded peak at ~2.6-2.7 ppm. The small number of amino hydrogens on the ends of each polymer strand should account for ~3.5-3.7 ppm. The tallest peak within both spectra is at ~7 ppm, accounting for the aromatic hydrogens on the imidazole groups. Further, the small shifts that have separated from the more prominent peaks in the Os-PVI spectrum following at 7.44 ppm and 8.24 ppm represent the hydrogens on imidazole groups that have been de-shielded due to the high electron density of osmium coordination at this position.[38] This indicates $Os(bpy)_2Cl_2$, or rather $[Os(bpy)_2Cl]$, has bound to the polymer. In the f-Os-PVI spectrum, a much smaller peak follows at 7.57 ppm. The magnitude of this peak suggests that the osmium precursor had not bound as efficiently to the polymer backbone.

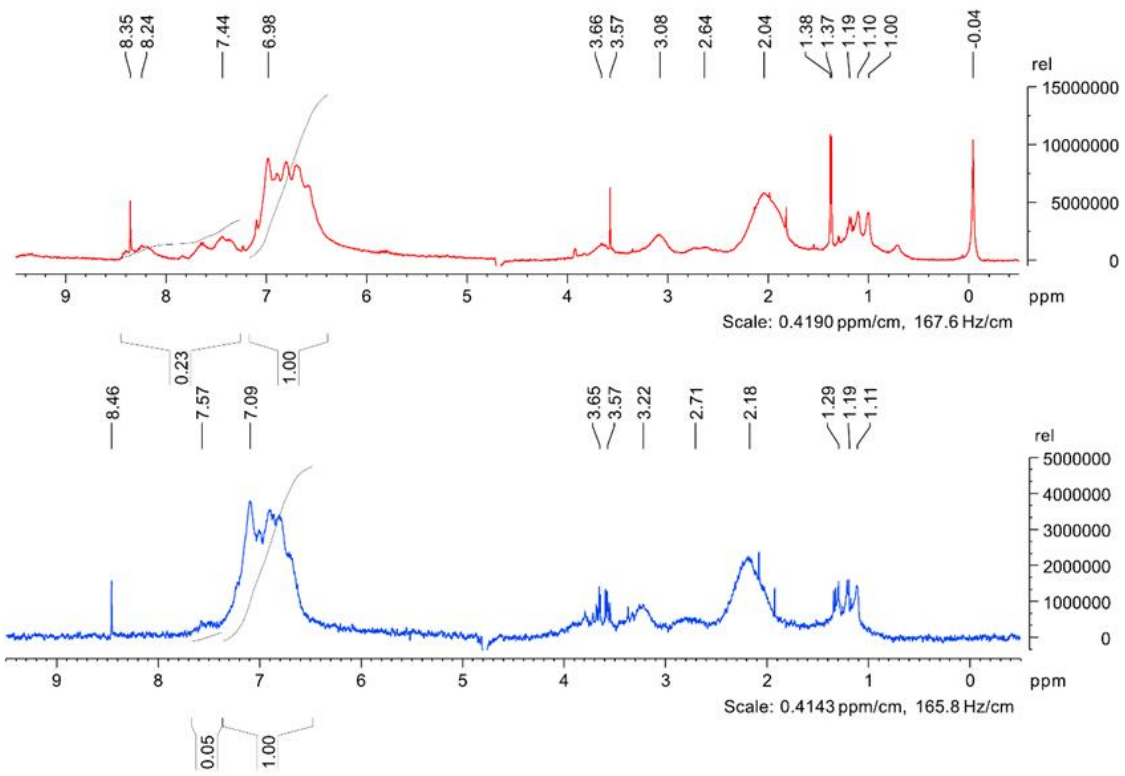

Figure 3.3. ^{1}H NMR Spectra Os(bpy)$_2$Cl-PVI (Red), and f-Os-PVI (Blue). As shown, the 0-6 ppm shifts in the two spectra show similar characteristics of the PVI backbone. In the ~ 7 ppm shift range, indicate the broad peaks of the imidazole side chains. The differences appear from approximately 7.2-8.5 ppm. The Os-PVI shows the downfield shifts of osmium-bound imidazole. The f-Os-PVI spectrum shows a further shift of the base imidazole peak due to the oxygen determined to be in the product.

Metal loading, the amount of the organometallic precursor, bound to the polymer backbone, can be estimated via NMR integrals.[37] By setting the peak of the imidazole to 1.00 and adjusting the ratios for the osmium shifted peaks accordingly, we can then utilize the following equation to determine the approximate metal loading of the polymer overall.

$$Approximate\ Metal\ Loading = \frac{osmium-affected\ proton\ integrals}{normalized\ (to\ 1)\ imidazole\ proton\ integral + osmium-affected\ \ proton\ integrals} \times 100\% \qquad \textbf{Equation 3.1}$$

For example, during the processing of the ^{1}HNMR spectrum for Os-PVI, the integrals for the imidazole protons and the osmium-affected protons were picked. The imidazole peak integral was set to 1.00, and the software automatically adjusted the value of the osmium-affected protons to 0.23. Using these two values, we estimated the metal loading for the batch of Os-PVI utilized in these experiments.

$$Approximate\ Metal\ Loading = \frac{0.23}{1.00+0.23} \times 100\% \approx 20\% \qquad \textbf{Equation 3.2}$$

To summarize, the Os-PVI has an approximate metal loading of 20%, and the f-Os-PVI has an approximate metal loading of 5%. Since the concentrations of the Os-PVI and f-Os-PVI samples were the same, we can directly compare the two. The f-Os-PVI did not load as much osmium onto the polymer backbone as the Os-PVI, according to this NMR, consistent with the extra oxygen coordination around the Os center in f-Os-PVI inhibiting attachment to the PVIAA backbone.

Fluorescence

Oxygen contamination of the organometallic polymer gave rise to a unique luminescent property not previously seen in Os redox polymers. For the fluorescence of the organometallic polymers when excited in the UV (360nm) region, the f-Os-PVI could emit light in the visible spectrum. At the same time, the Os-PVI was not (figure 3.4). Compared to the original PVIAA backbone, the fluorescence has been significantly quenched and slightly red-shifted (approximately 25nm). While the quenching data alone supports a lower loading amount of the organometallic onto the polymer backbone, the color shift also confirmed a change in the energetics of the emission.

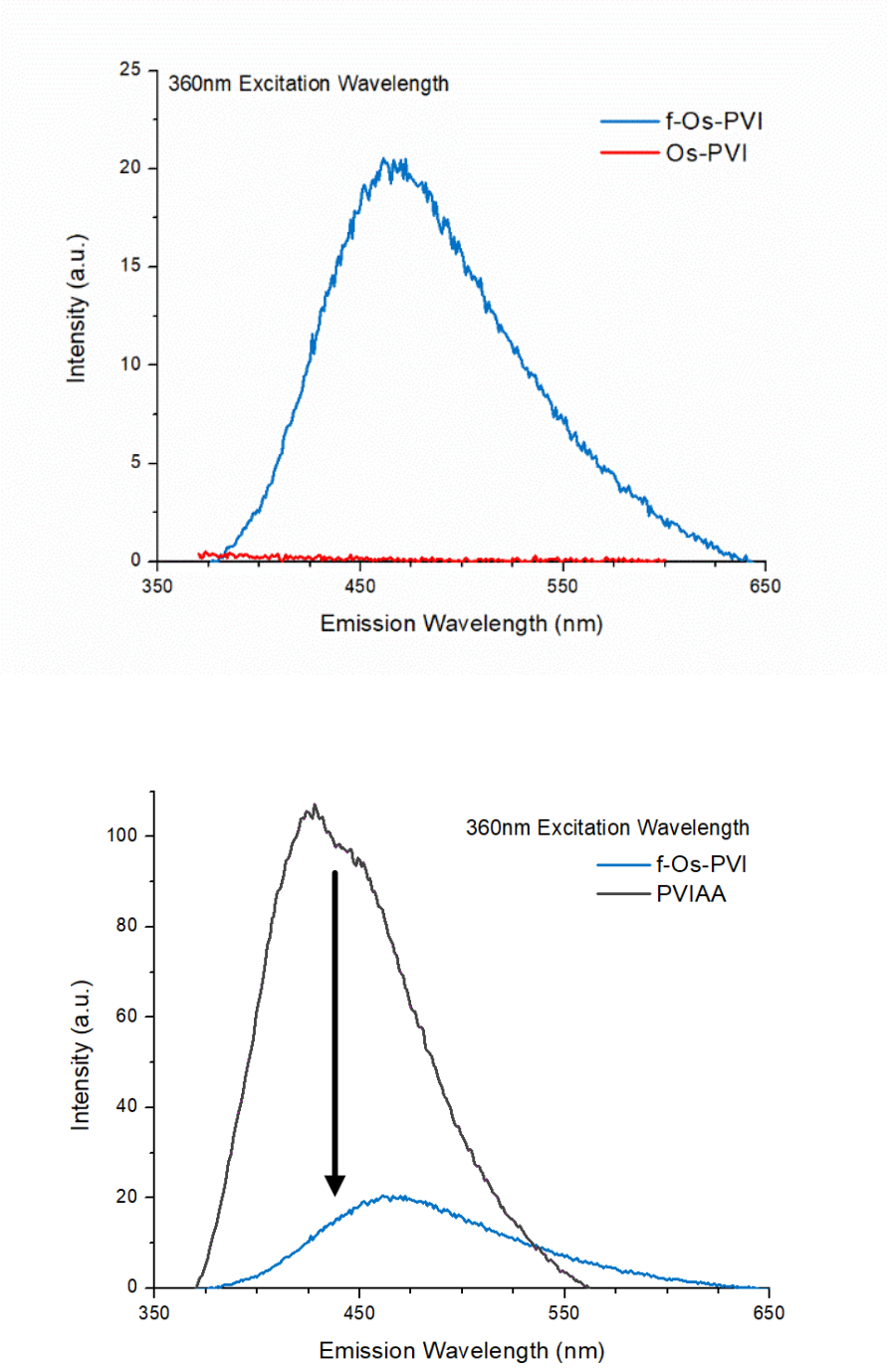

Figure 3.4. Fluorescence Emission Spectra for PVIAA, Os-PVI, and f-Os-PVI. The Os-PVI (red) does not demonstrate light emission (top). Attaching the f-Os precursor to create f-Os-PVI (blue) quenches the baseline light emission from the PVIAA backbone (black) and shifts the wavelength from approximately 430 nm to 475 nm (bottom).

Cyclic Voltammetry

The Os-PVI had an $E_{1/2}$ of +0.15 V vs. Ag/AgCl, which is expected of this polymer-based on literature values and its usefulness in Type II oxidase biosensors.[39] The NMR and fluorescence data above suggest that the osmium did attach, and the CV supports this as the other organic compounds in the solution are not redox-active. However, attachment of the f-Os precursor to the polymer backbone shifted the $E_{1/2}$ to +0.5 V vs. Ag/AgCl, reflecting the Osmium center's oxygen coordination shifting its oxidation to more positive potentials (figure 3.5). Unfortunately, this sizeable positive shift no longer allows for this redox polymer to be useful for oxidase enzyme-based electrodes; it may be helpful for electrochemical mediation for other enzymatic co-factors needing more positive potentials.

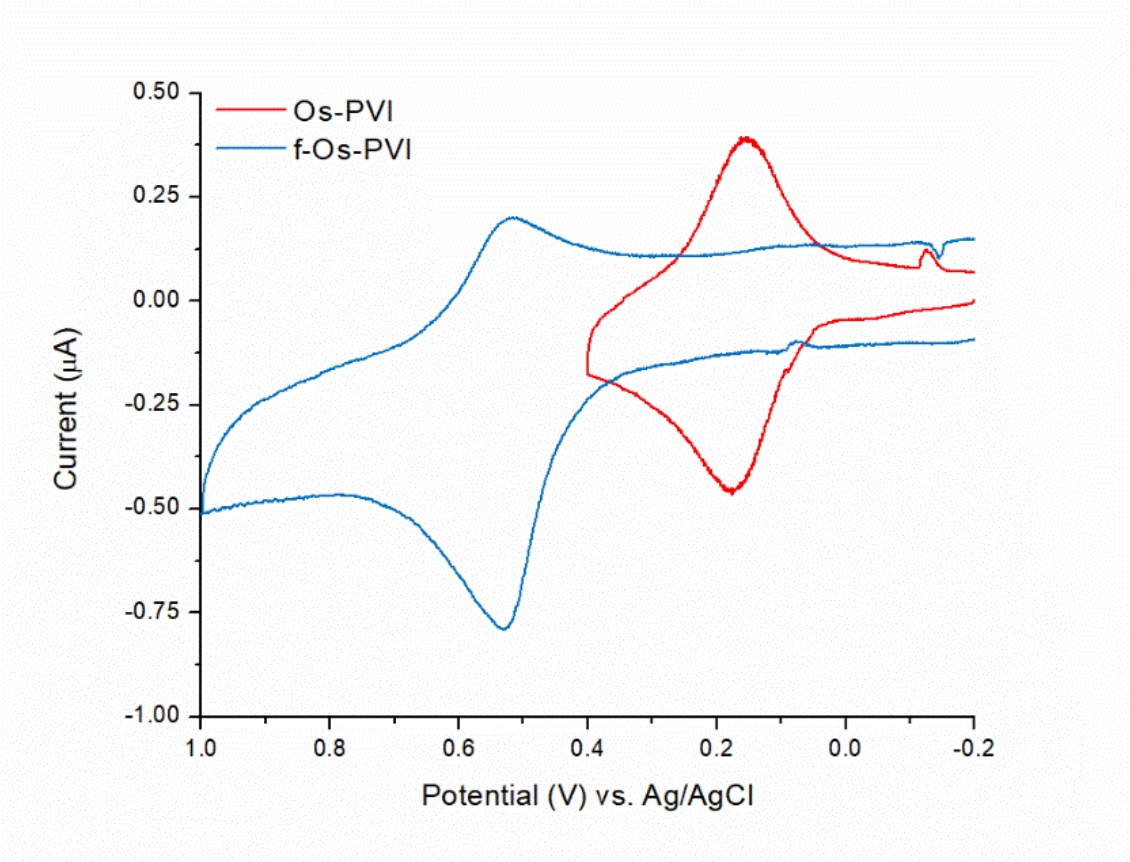

Figure 3.5. Cyclic Voltammograms of Os-PVI (red) and f-Os-PVI (blue). The cyclic voltammogram characterization for each of the polymers demonstrates their electrochemical reversibility. The Os-PVI i_p are approximately equal, and the ΔE_p suggests electrochemical reversibility. The f-Os-PVI has a distinct difference between the cathodic and anodic current peak heights, providing evidence of ease in electron transfer during oxidation and difficulty during reduction.

Trace oxygen exposure during $Os(bpy)_2Cl_2$ synthesis provides mixed yields of $Os(bpy)_2Cl_2$ along with $Os(bpy)_2O_2$. Once incorporated into the polymer, the OsO_2 polymer has an $E_{1/2}$ that is more positive, enabling more interference and requiring higher overpotential to detect at the electrode. This makes the OsO_2 polymer an unsuitable choice for biosensors. Since both compounds will bind to the backbone polymer, it is important to minimize oxygen contamination to maximize the end yield of the efficient Osmium polymer.

3.1.4. Conclusions & Future Outlooks

We have shown that oxygen contamination for the synthesis of $Os(bpy)_2Cl_2$ will lead to low yields of the desired intermediate and a completely different Os complex, $OsO_2bpy_2Cl_2$. This compound is hard to distinguish from its original counterpart during the synthesis. After mass spectrometry, NMR, luminescence, and electrochemical characterization were distinguished, the role of trace oxygen during the intermediate synthesis was determined. This oxygen-containing complex and its resulting redox polymers demonstrated reversible electrochemical behavior but cannot mediate electron transfer in oxidase enzyme wired electrodes. In the future, this new redox polymer may be helpful for electrochemical mediation at its higher potential for other enzyme systems.

4. STATIC AND MICROFLUIDIC INDIRECT COMPETITION ENZYMATIC ELECTROCHEMICAL IMMUNOASSAY (icECIA) FOR INTERLEUKIN-6

Chapter 4 investigates attempts towards an adaptable, customizable immunoassay for static and microfluidic systems for cytokines, beginning with Interleukin-6 (IL-6). A method for both the static sensor and microfluidic system was developed. The optimization of the individual components, starting with the electrochemical signal compound *p*-aminophenol (PAP), is discussed in this chapter. Thank you to Kody Wolfe, Olivia Owens, and Hawkins Shephard for their assistance in collecting this data.

4.1. Optimal *p*-aminophenol Concentration Determination for Multi-platform Early Sepsis Intervention Biosensor

4.1.1. Introduction

IL-6 is a pro-inflammatory cytokine that assists in the body's natural immune response. Often used as a biomarker, IL-6 is used as a signal of tissue repair for systemic inflammatory response syndrome (SIRS), sepsis, and more recently, COVID-19.[40-42] The out-of-control immune response that can come with these diseases and others that involve IL-6 leads to the desire for a rapid, low-cost test that would allow for easy detection of IL-6 blood concentrations. This would allow for easy bedside diagnosis with clinicians and patients knowing when to seek hospitalization.

For example, with sepsis, the overwhelming immune response leads to organ failure. The mortality rate following organ failure is exceptionally high.[43-44] Since sepsis appears symptomless or masquerades as other issues post-operatively, it is often discovered when symptoms of significant immune response and organ failure appear. It is often too late to get the infection under control at this stage. Early intervention of sepsis would require detection of the immune response earlier in the process.

The IL-6 blood concentration is consistently between 0 – 2000 pg/mL as past 1000 pg/mL death is likely to occur in patients. As IL-6 concentrations indicate tissue repair, extremely low concentrations of IL-6 (below 100 pg/mL) are not clinically relevant. These are parameters that biosensors should take into account during the design process.

IL-6 Sensors

A 2020 IL-6 review discussed a variety of electrochemical. Since IL-6 is a protein, the best method for an assay is electrochemical detection due to the high level of sensitivity it brings, necessary for a clinical test. However, IL-6 is electrochemically inactive, like most proteins, requiring the use of an electrochemical immunoassay or ECIA. Additions to this acronym can be added depending upon the specifics of the types of assays being discussed. There are three main subcategories to ECIA sensors: direct ECIA (dECIA), indirect competitive (icECIA), and sandwich ECIA (sECIA).[45]

dECIA strategies produce their signal from the interaction of the analyte with the antibody immobilized on the electrode surface, typically via a self-assembling monolayer (SAM). Electron impedance spectroscopy (EIS) is often utilized with this type of sensor, and aptamers also fall into this category. Nano components can be used to amplify the signal.[46-48]

icECIA has the signal compete with the analyte for the binding receptor. This is usually done by taking the target analyte, binding it to the signal compound, and dosing it as standard in calibrants and samples.[45] Higher concentrations of the analyte will displace more of the target-signal complex yielding a lower signal, producing an inverse relationship.[49] This technique is utilized in this work.

sECIA uses a second antibody, completing the “antibody sandwich”. Two labels are usually used in electrochemical biosensors, nanoparticles, and enzymes. The enzyme most

commonly used is the combination of horseradish peroxidase with streptavidin and biotin to detect hydrogen peroxide. Overall the addition of this second antibody can help improve the limit of detection (LOD), specifically with low concentration sensors for cancer diagnostics.[45]

In Table 4.1, twelve citations are listed discussed in the review. These papers either include dynamic ranges that are not biologically relevant for IL-6, include electrochemical techniques that are not suitable for analytical electrochemistry, or are not replicable.

Papers in the field of IL-6 are interested in publishing the sensor work they have as opposed to whether or not it yields a path towards a suitable sensor for a clinically-relevant IL-6 sensor.

Detection Method	Technique	Analyte & Conjugate	LOD †	Dynamic Range †
Direct ECIA	CV, EIS, DPV ✘	IL-6	20	20–100 ✘
Direct EC aptasensor assay	CV, EIS ✘	IL-6	0.33	1–15,000,000
Direct EC aptasensor	FET	IL-6	1	1–100 ✘
Direct ECIA	LGFET	IL-6	1.37	1–100 ✘
Indirect competitive ECIA	EIS, LSV ✘	PS/PDA/AgNP/IL-6	0.059	0.1–100,000
Direct ECIA	EIS ✘	IL-6	0.00001	0.00001–0.1 ✘
Sandwich ECIA/NP	CV, DPV	TiP/AgNP/ Ab_2/IL-6	0.1	0.00001–10,000
Sandwich ECIA/NP	CV, SWV	FC/PPN/ Ab_2/IL-6 ✘ Not replicable	1	2–20,000
Sandwich ECIA/NP	CV,(SWV)	CTAB(AuNP)/ Ab_2/IL-6	2	5–50,000
Sandwich ELECIA	Amperometry	S1-Avidin/Biotin-Ab_1 (+) S2-HRP-S3(TargetDNA)	0.05	0.2–20 ✘
Sandwich ELECIA	EIS, Amperometry ✘	CNT/PDA/AuNP/ Ab_2-HRP-IL-6	1	4–800 ✘
Sandwich ELECIA	Rotating Disc Amperometry	Ab_2-Biotin/(m)HRP-Streptavidin/(h) Ab_2-MWNT-HRP	0.5	0.5–30 ✘

† mentioned in pg/mL.

Table 4.1. Compilation of IL-6 ECIAs. From Khan *et al.*, this lists the various detection methods, electrochemical techniques used, and the dynamic ranges. Red X's indicate either an unsuitable analytical technique was used, an irrelevant biological range for IL-6 was reported, or the results were not replicable by the author of this disseratation.[45]

Alkaline Phosphatase Use and AP/PAP Sensors

Alkaline phosphatase (AP) is an enzyme that cleaves a phosphate group from the compound upon which it acts.[50-51] It works optimally at pH 9; however, it can function at pH 7.4, the pH most often found in the body.[52] Often, AP is used as a tag for biological research. It is

expressed in cells or tagged onto oligonucleotides.[53-55] Within the last 25 years, AP has been used in combination with 4-aminophenyl phosphate (also known as *para*-aminophenyl phosphate, PAPP) to create the basis for an electrochemical biosensor platform.[56-57] Together, this pair with an antibody and antigen combination can form an icECIA. PAPP is electrochemically inert until its phosphate group is removed, transforming it into 4- or *para*-aminophenol (PAP). PAP is electrochemically active and available to be oxidized by the electrode upon which the sensor is built. Multiple papers have built sensors around this idea. However, the lack of inclusion in the sensor review for IL-6 shows that it is not a commonly used sensor for the IL-6 community (although it can be acknowledged that no review can be exhaustive).[58-59] Several additional uses for the AP/PAPP combination are explicitly used for PAP or PAPP. These compounds are considered toxic, and sensors for them can be regarded as useful.[60-62]

PAP Electrochemical Characterization and Polymerization

4- or *para*- aminophenol as a compound has been studied electrochemically both theoretically and experimentally. There are two agreed-upon reaction schemes for the redox of PAP.

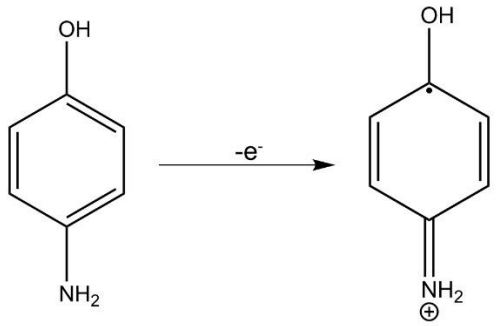

Scheme 4.1. PAP one-electron transfer.

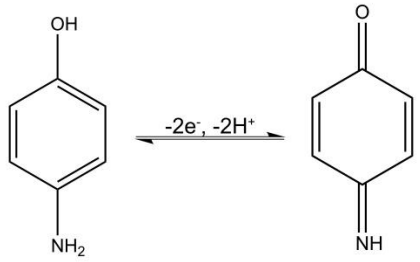

Scheme 4.2. PAP two-electron, two proton transfer.

Scheme 4.1 shows the one-electron electrochemistry that creates a radical electron believed to be responsible for electropolymerization.[63] Scheme 4.2 is the two-electron two proton process that makes PQI demonstrated by Yin *et al*.[64] Both of these reaction schemes were verified by Wang *et al*. using spectro-electrochemistry in acetonitrile.[65]

There is a gap in the PAP literature for thorough characterization in biological conditions. Many list the purpose of their investigations due to PAP and other aminophenols being toxic side products in manufacturing processes or with xenobiotics. Several list acetaminophen, or paracetamol. The typical pH in the human body is pH 7, with the blood specifically being within the range of 7.35-7.45.[66] Outside of this range, the blood is drifting towards being considered acidic or alkaline, with metabolic acidosis being officially defined as pH 7.00 and lower.[67] Metabolic acidosis due to chronic use of paracetamol is where doctors are primarily concerned therefore studying this compound outside of biologically relevant pH is non-necessarily of relevance for that community.[68-69]

Nematollahi *et al.* studied the electrochemical oxidation of PAP at many pH values and scan rates; however, they did not focus on the pH values in the liver.[70] This is where they found dimerization to occur, and therefore pQI and pBI were not present, the byproducts of concern.

Beiginejad *et al.* studies at pH 5 only again out of the pH window we find to be biologically relevant.[71]

Chandrashekar *et al.* studied PAP in a combination of ethanol and water (1:10 due to the concentrations of their stock to final concentrations of the analyte).[72] Despite utilizing a solvent mixture, they found an additional anodic peak that was adsorption controlled with a scan rate study. They used concentrations 1mM to 4mM PAP.

Taj *et al.* attempted to create a new electroactive polymer in the form of poly(PAP) for potentiometric sensors. At the time, polyoxophenylenes and polyanilines were popular in being studied but were not soluble in non-organic solvents. It was demonstrated that this could form a film on an electrode surface, with CVs in methanol and aq. HCl.[73]

For this project, an icECIA was developed to work statically in a container or well and a microfluidic environment (figures 4.1 and 4.2). For both assays, the analyte protein IL-6 is bound to AP. If PAPP and AP are combined into a solution, and PAP's $E_{1/2}$ of 0.02V (vs. Ag/AgCl) is applied, any current detected will be from AP producing PAP from the PAPP supply.

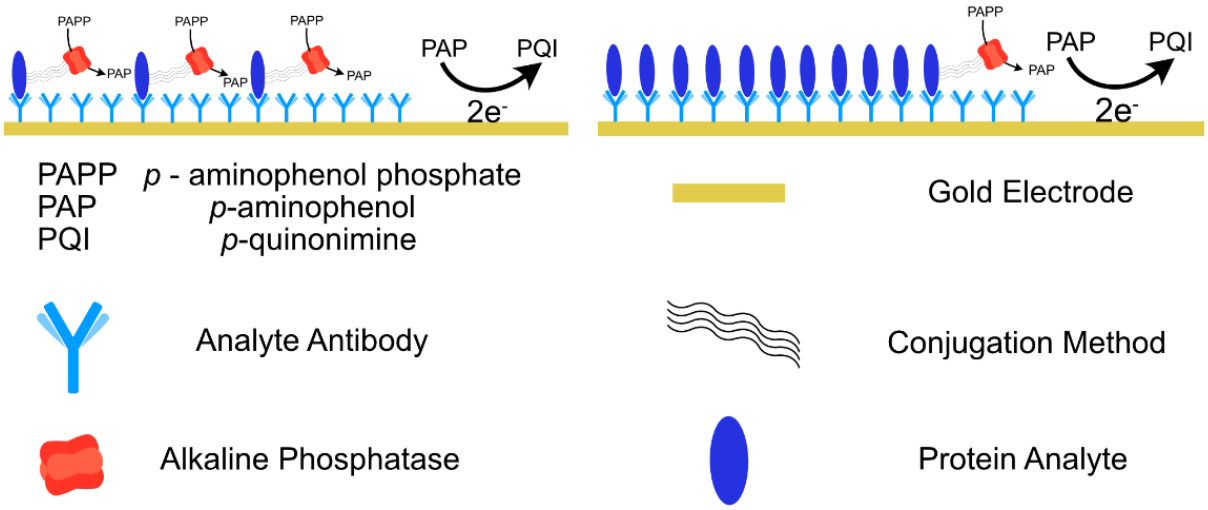

Figure 4.1. Static Protein PoC Sensor. Antibodies immobilized on a gold SPE capture protein analyte bound via kit conjugation method to AP. AP turns over electrochemical inactive PAPP into electrochemically detectable PAP. This creates the baseline for a competitive assay. Diluting the AP bound protein analyte with unconjugated protein analyte, either from calibrant concentrations or patient sample, competes for antibody positions. This limits the amount of local PAPP turned into PAP and drops the amount of electrochemical signal detected.

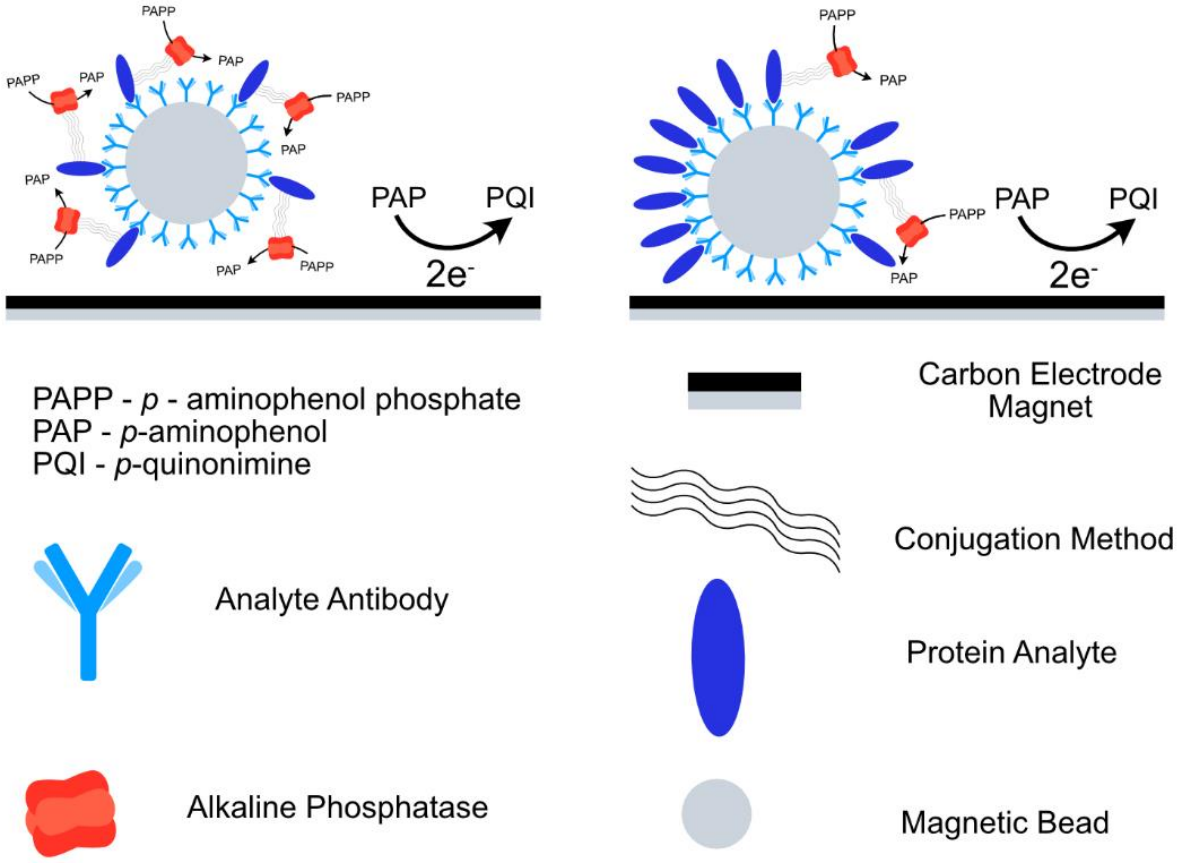

Figure 4.2. Microfluidic Protein Sensor for OoC. The microfluidic sensor is similar in design to the static sensor. A competitive assay utilizes the protein analyte conjugated to AP as the baseline, with the unconjugated protein analyte competing in calibrants and samples to fluctuate the PAPP/PAP turnover signal. The difference comes from the location of the antibodies, which are immobilized on magnetic beads. The magnetic beads are held over a carbon electrode with a magnet outside the microfluidic housing that can be placed and removed, allowing the beads to be washed away at the end of a calibrant or sample.

A baseline first needs to be created with these sensors. This is done by capturing a set concentration of IL-6 protein covalently bound to AP enzyme with IL-6 Ab_2 on an electrode surface. Once this baseline is set, a new sensor is exposed to the unknown sample of IL-6, dosed with the baseline concentration of IL-6/AP used previously. The IL-6 in the sample will compete for antibody binding positions with the IL-6 bound to the AP. However, the IL-6 in the sample will not convert PAPP to PAP, creating the electrochemical signal. This signal dilution can back-calculate the sample concentration throughout several different sample ratios to IL-6/AP.

During the development into static and microfluidic versions of this sensor, the PAP needed further electrochemical characterization.

4.2.2. Materials and Methods

Chemicals

KCl (Certified ACS) and 7.4 pH phosphate buffer solution (Certified ACS) were obtained from Fisher Scientific. The following chemicals were obtained from Sigma Aldrich: *para*-aminophenol (≥98%), *para*-aminophenyl phosphate (monosodium salt; ≥98%), 6-mercapto-1-hexanol (MCH; Sigma ≥97%) ethanolamine hydrochloride (Sigma ≥95%). IL-6 Mouse anti-Human antibodies (monoclonal, Clone: 1936, unconjugated) and IL-6 Protein (Recombinant Human, Carrier Free) were obtained from R&D Systems. 11-mercaptoundecanoic acid (MUA; Santa Cruz Biotechnology ≥95%) was from Santa Cruz Biotechnology. The Alkaline phosphatase Conjugation Kit - Lightning-Link® (Abcam #ab102850) was from Abcam. DI water (18.2 MΩ) was used when necessary.

Solution Preparation

A stock of 1 mM PAP was created by dissolving solid PAP into a solution of 2 mM KCl and 120 mM 7.4 pH phosphate buffer (PBS). This stock was then used to create the 1000 µM PAP

solution, and a serial dilution then took place to make the other solutions for analysis: 200 µM, 400 µM, 600 µM, and 800 µM. The KCl/PBS solution was either a background or blank, depending on the experiment. These solutions were always made fresh each day are used consistently in the experiments unless otherwise stated.

UV-Vis Spectrometry

Absorption experiments were performed on Cary 50 Bio in Dual Beam mode. Scans were performed from 800 nm to 200 nm to determine the locations of the absorbance peaks. The scans were then narrowed to 400 nm to 200 nm. Data was collected in 0.50 nm steps.

Microfluidics and Chronoamperometry

The microfluidics consisted of a peristaltic pump, a 24-port valve, gas-liquid filter debubbler, and 26-µL electrochemical cell. These were designed and fabricated by VIIBRE at Vanderbilt University. A CH Instruments 900D Bipotentiostat and screen-printed electrodes (SPEs) from Pine Research Instrumentation with a 2 mm OD gold working electrode, a Ag/AgCl reference electrode, and a gold counter electrode were used to perform the amperometric experiments. The amperometric i-t curve was performed by holding the working electrode at +0.3 V (vs. Ag/AgCl) with sampling every 3 seconds.

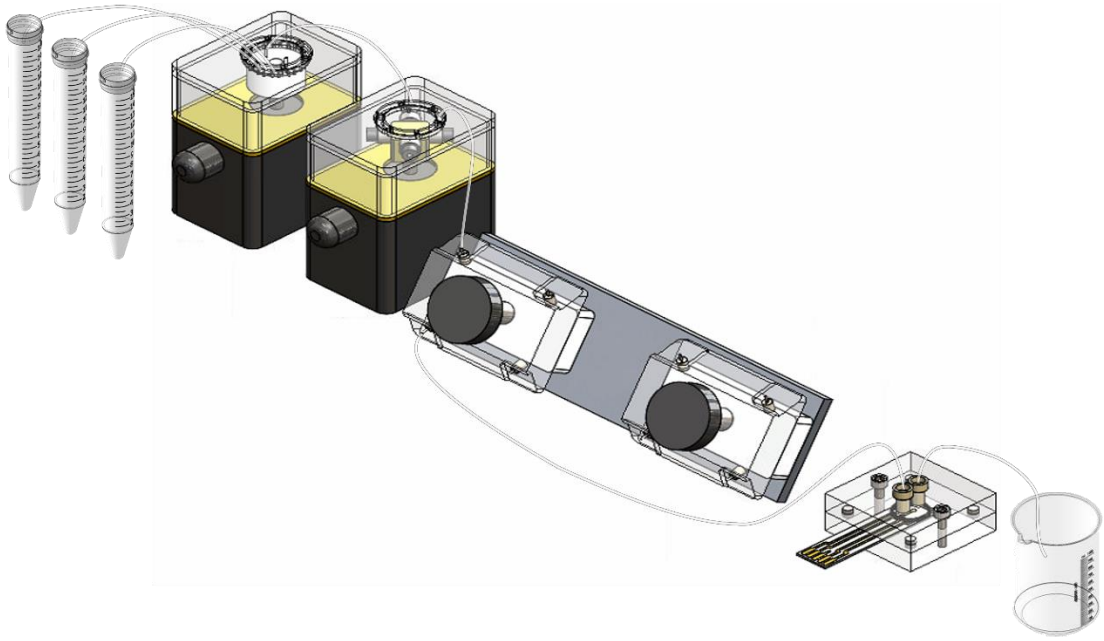

Figure 4.3. Complete Microfluidic System from solutions to SPE to waste. Moving from left to right solution begins in volumetric centrifuge tubes, then pulled 24-port valve by the peristaltic valve. The solution is then moved into the debubbler with a gas-liquid membrane before entering the housing that holds the SPE and the 26 µL electrochemical cell. The solution then exits the housing into the waste beaker. Picture courtesy of Breck and Olivia Owens.

Cyclic Voltammetry

CH Instruments 900D Bipotentiostat and screen-printed electrodes (SPEs) from Pine Research Instrumentation with a 2 mm OD gold working electrode, a Ag/AgCl reference electrode, and a gold counter electrode. All cyclic voltammograms were run the same, starting with an initial voltage of -0.2 V (vs. Ag/AgCl), then to +0.3 V, and back to -0.2 V at a scan rate of 0.1 V/s and a 1×10^{-6} sensitivity. This was performed for 30 segments (or 15 cycles). The first cycle is the "first scan" and the last cycle is the "last scan" for each concentration.

The CV experiments had more concentrations tested than the other experiments; however, their samples were made in the same way, starting with a 1 mM stock solution in the KCl/PBS buffer then diluting to the 1000 µM concentration and performing serial dilutions from there to achieve the desired concentrations for analysis.

4.2.3. Results & Discussion

The various concentrations of PAP do not prove ideal for repeated electrochemical measurements. When evaluating a compound for its suitability as a redox tag in an electrochemical assay, multiple characteristics are considered: reversibility, Nernstian behavior, contaminants or side products, stability through repeated electrochemical testing. Stability specifically can relate to the increase of potential contaminants or side products and the potential for surface fouling. There is an increased probability of this with biological assays due to the likely adherence of proteins and other biological molecules to electrode materials (e.g., carbon and metals).

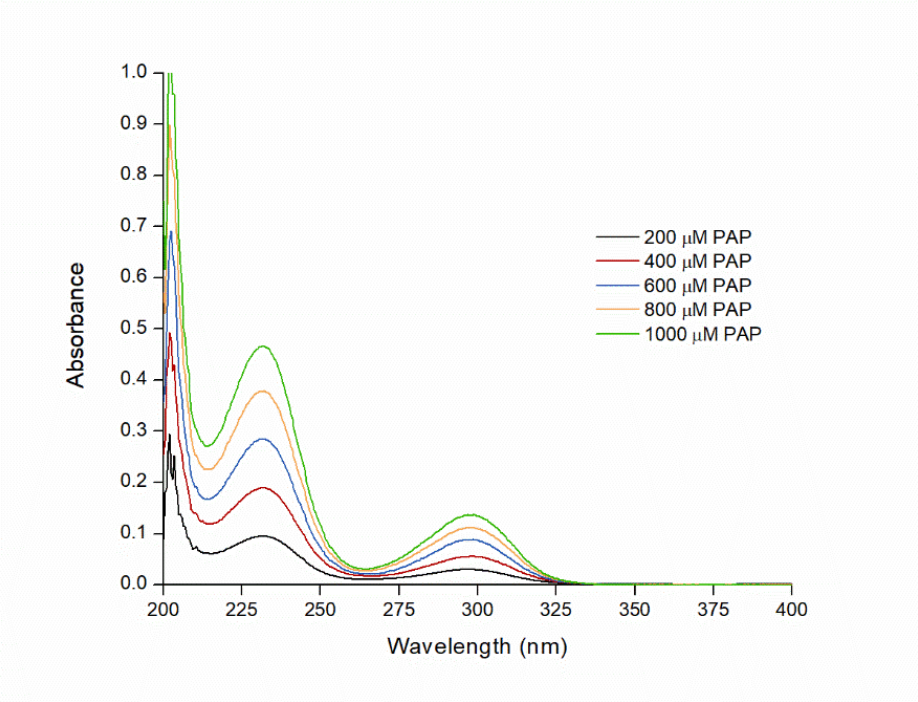

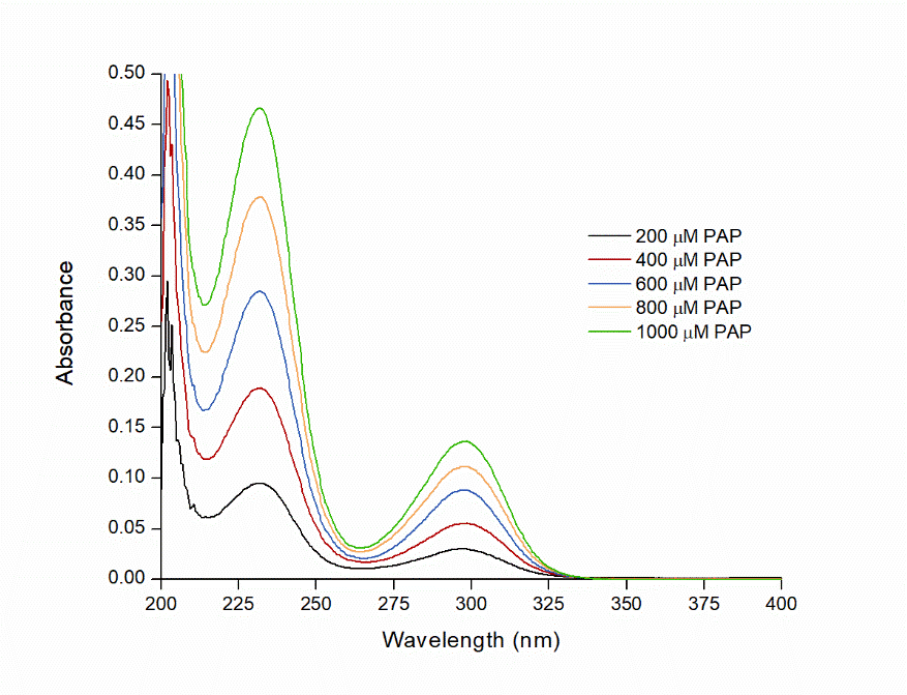

Figure 4.4. UV Vis Spectrometry of PAP concentrations 200 nm to 400 nm 0 to 1 Absorbance (top) 0.00 to 0.50 (bottom). Linearity appeared to be observed in both peaks at approximately 230 nm and 298 nm. The peaks at 298 nm were used for fit since they exhibited more gaussian behavior.

The linearity of PAP concentrations was compared between UV-Vis spectrophotometry and i-t amperometry within a microfluidic device. The absorbance peak at 298 nm was chosen due to its gaussian nature. The peak at 225 nm lifted on the blue shift side due to its proximity to the strong 200 nm absorbance. A group of 4 data points was picked where the peak appeared and averaged to give a peak absorbance. This was repeated with each of the concentrations, and a linear regression was performed once plotted. The R^2 value of 0.996 shows an agreement of 6linearity.

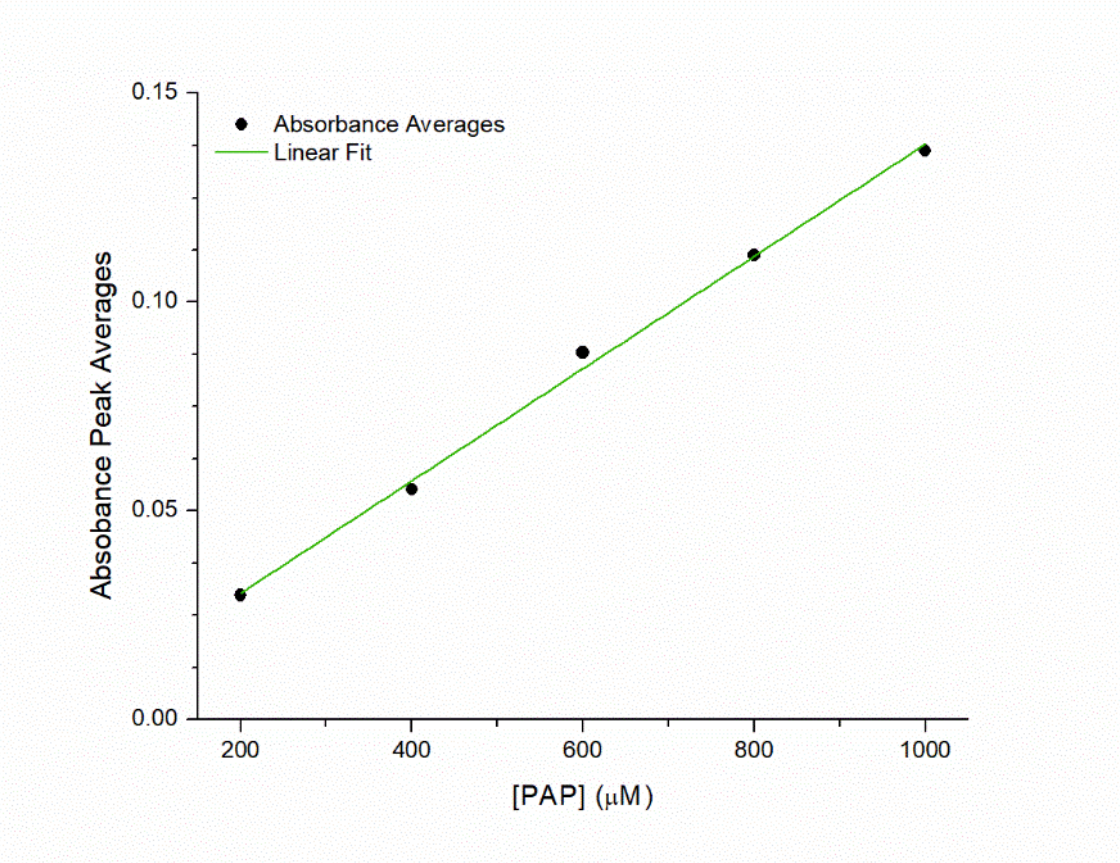

Figure 4.5. Absorbance Peak averages at 298 nm versus the concentration of PAP (μM). Peak heights (au) are the black data points, and the linear regression fit is the green line. The R^2 value of 0.996 shows an agreement of linearity amongst the data.

Each peak during an amperometric i-t run corresponds to a concentration of PAP being flown through the microfluidic device and over the electrode during that corresponding time. With each increasing concentration, an increase of the current response will occur. The raw data shown in figure 4.6 demonstrates this principle.

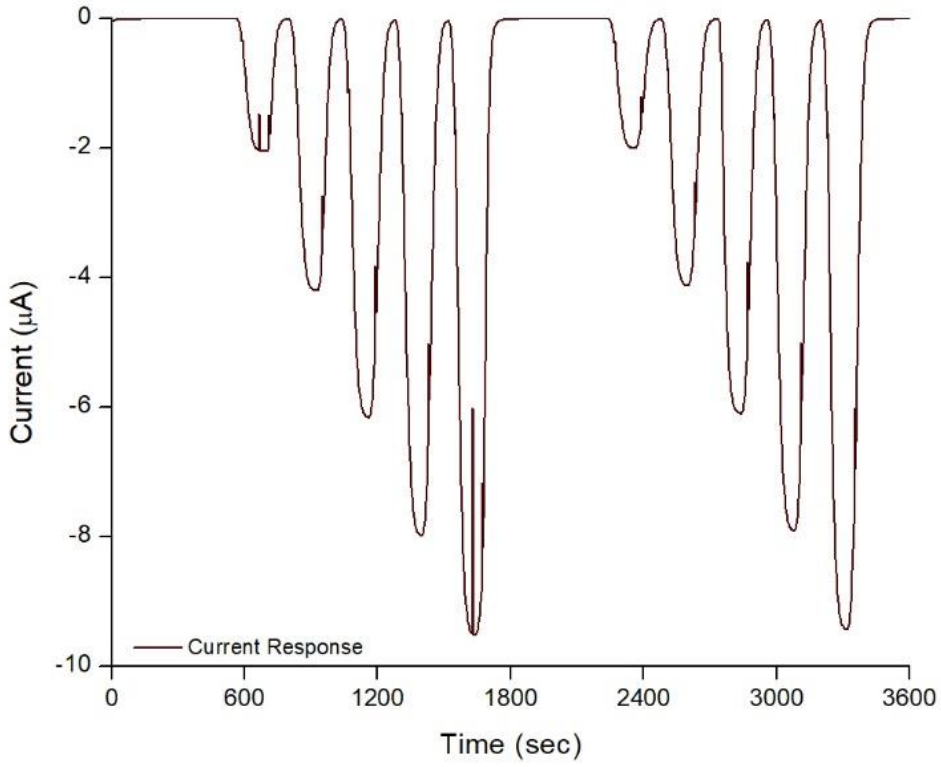

Figure 4.6. Amperometric i-t curve of PAP oxidation during microfluidic flow. Each peak demonstrates a concentration flowing through, with each taller peak being a higher concentration. PBS rinses were performed between each new concentration with a long PBS rinse between the two scans to ensure baseline was reached again before the initial lower concentration was re-run.

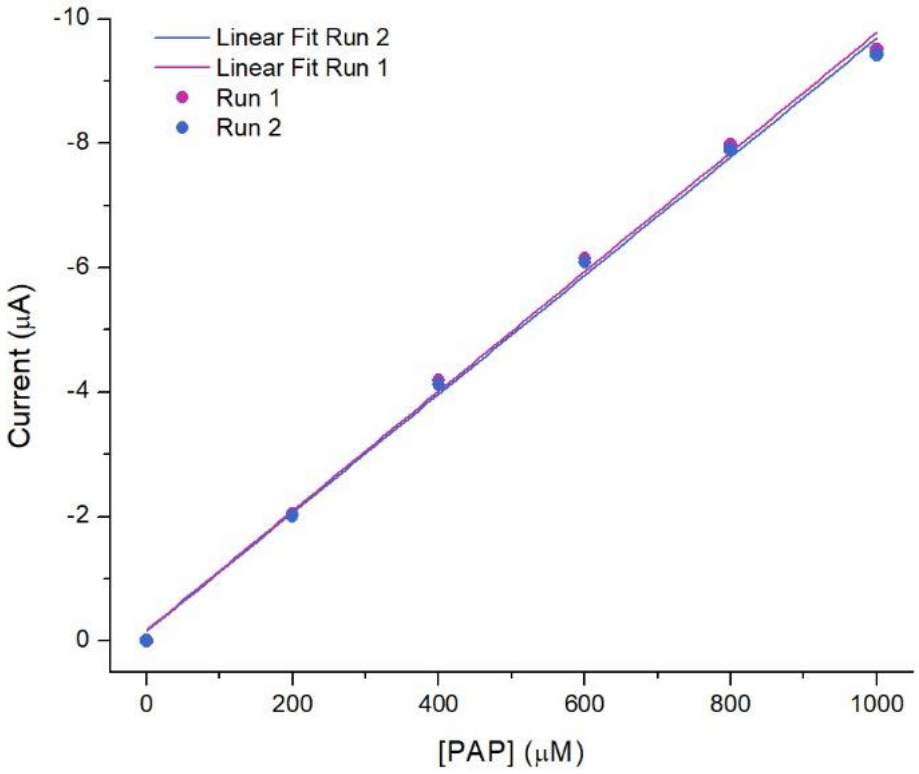

Figure 4.7. Current Peak averages versus the concentration of PAP (μM). Peak heights (μA) are points, and the linear regression fits are the lines. The R^2 values of 0.996 and 0.996 show an agreement of linearity amongst the data.

Runs were completed in addition to the ones found in figure 4.7. However, their data was incomplete (missing peaks, operator error). The peaks that were measured fell in line with the data shown above. When peaks are plotted (the same peak picking method is used as with the UV-vis), the same R^2 value is shown, demonstrating that linearity is still held for the PAP calibration curve when moved from a static measurement such as UV-vis to the flow method such as the microfluidic paired with the chronoamperometry. The difference in the slope values between the equations generated from the linear regressions demonstrates the sensitivity of the two techniques.

While this shows promise for the combination of PAP with flow chronoamperometry, more replicates need to be performed, ensuring this value holds.

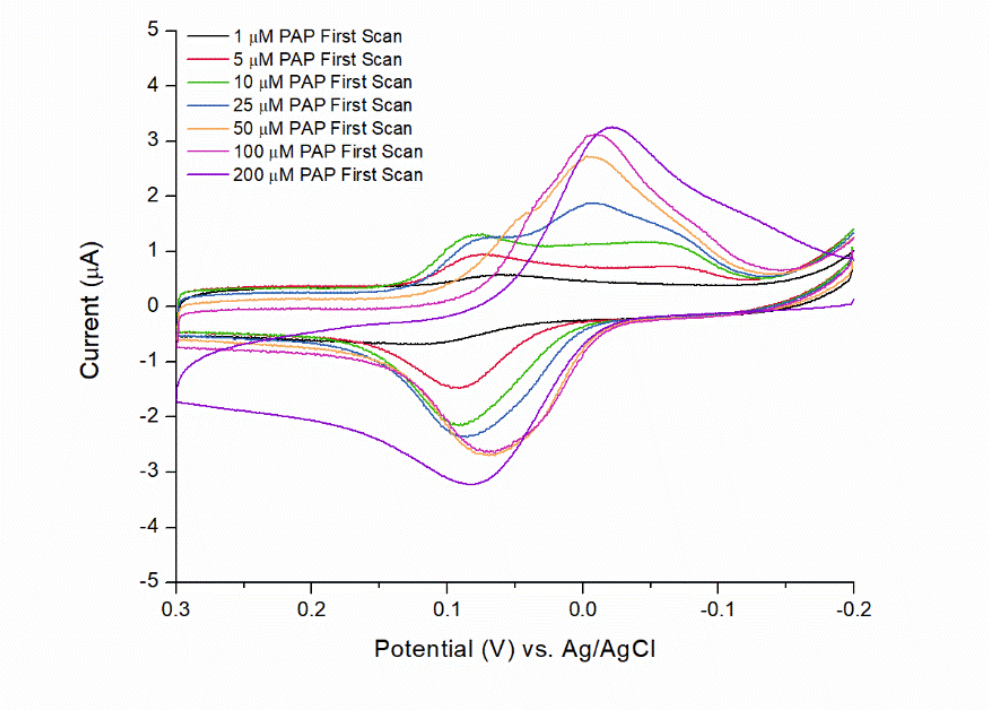

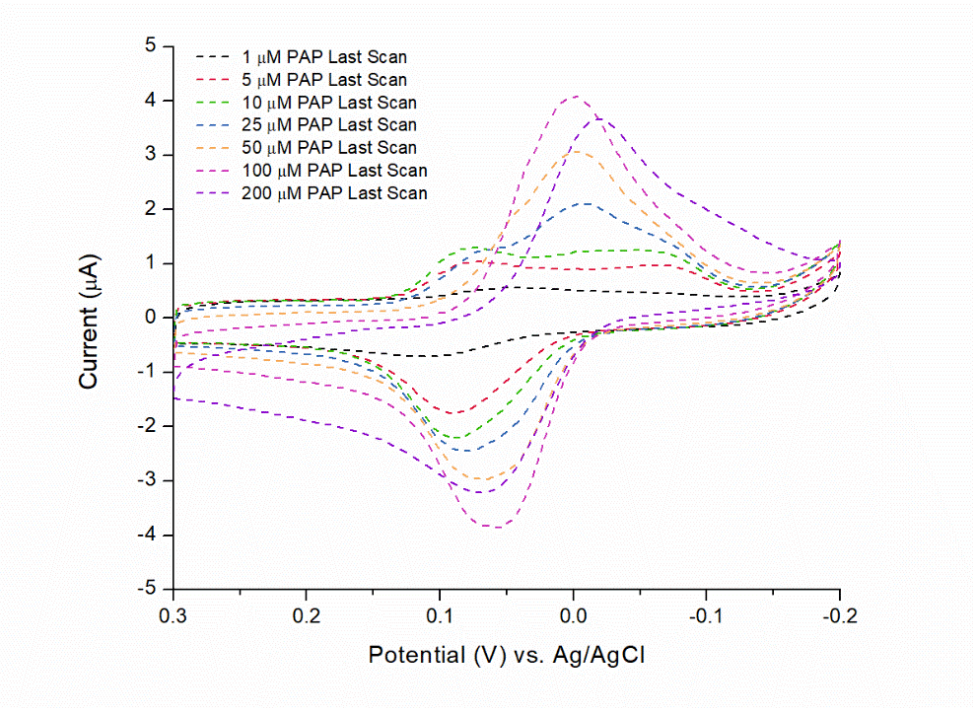

Figure 4.8. First Scan and Last Scan of 30 leg cyclic voltammogram cycle for multiple PAP concentrations. As the PAP concentration increases, two distinct reduction peaks merge into one, and the oxidation peak grows in height. The ipa and ipc increase for all concentrations between the first and last scans.

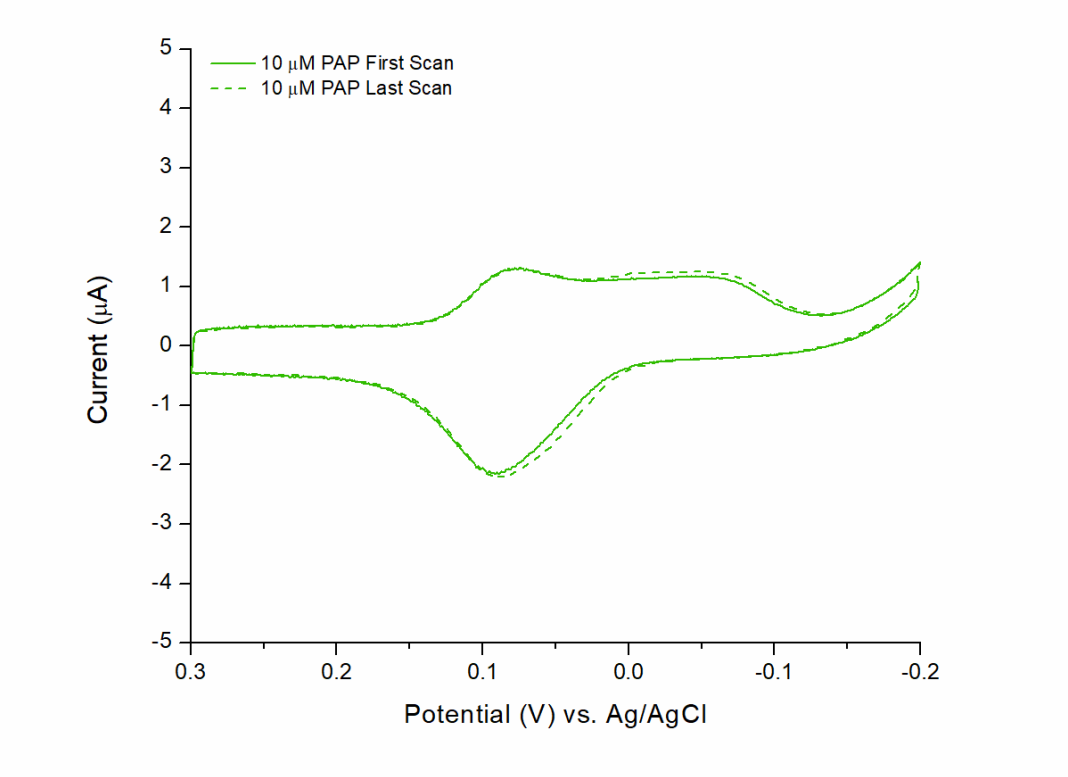

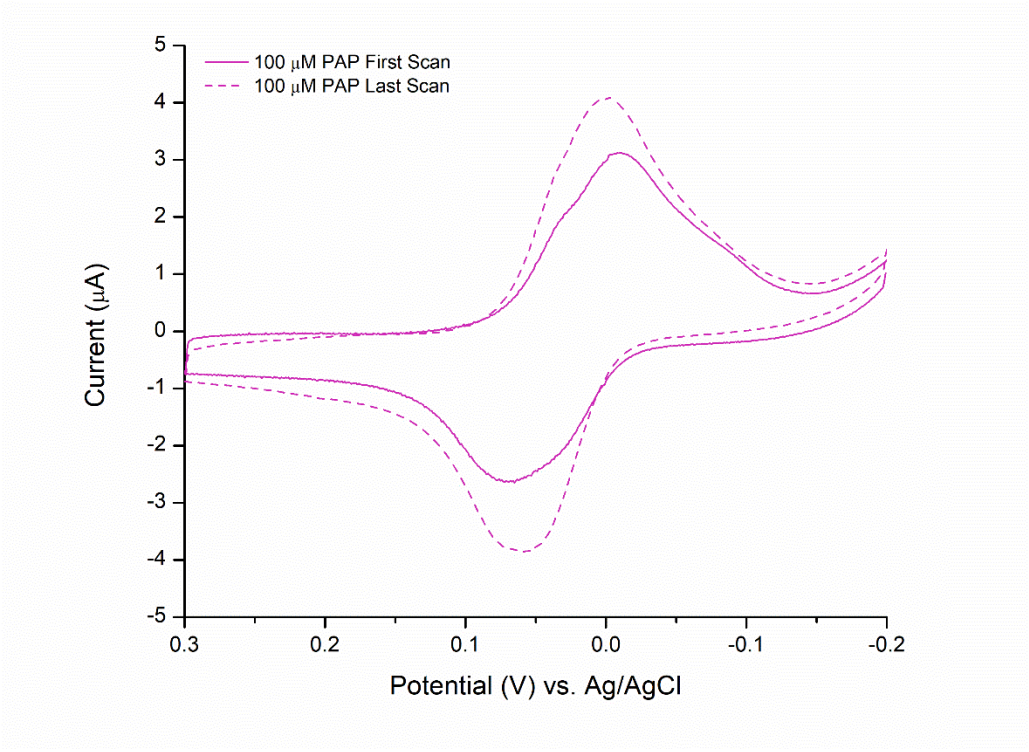

Figure 4.9. Overlays of 10 µM and 100 µM PAP of the First and Last Scan Cyclic Voltammograms. The increase in i_{pa} and i_{pc} is more apparent in these graphs, and the proportion of growth seems to scale with the concentration.

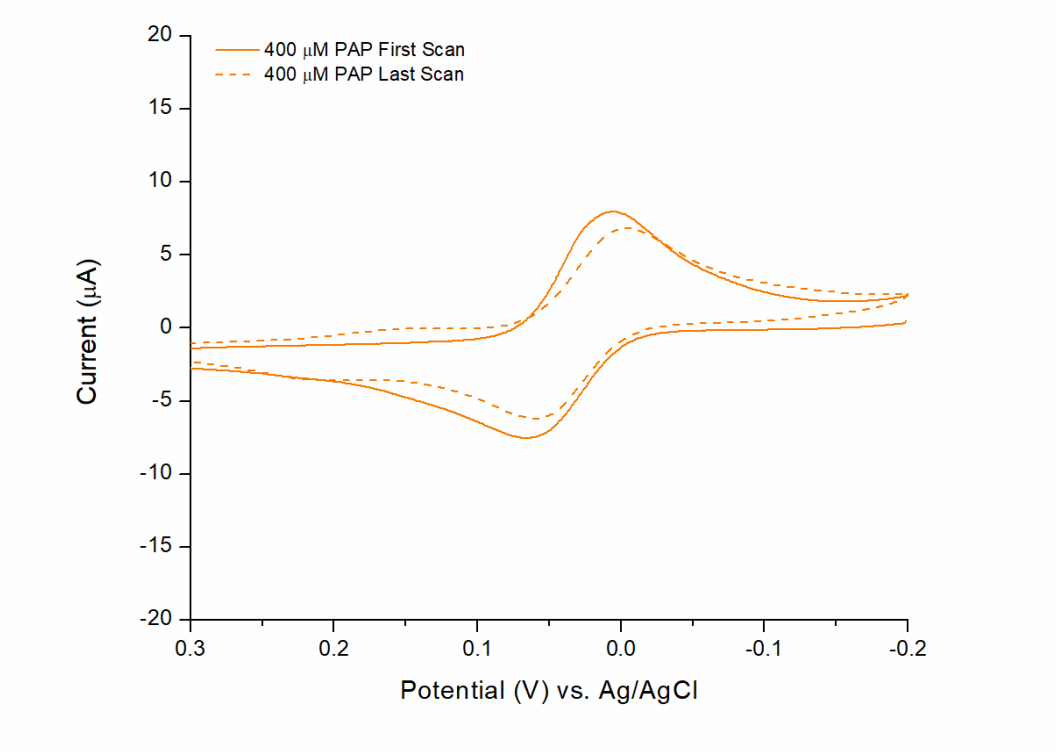

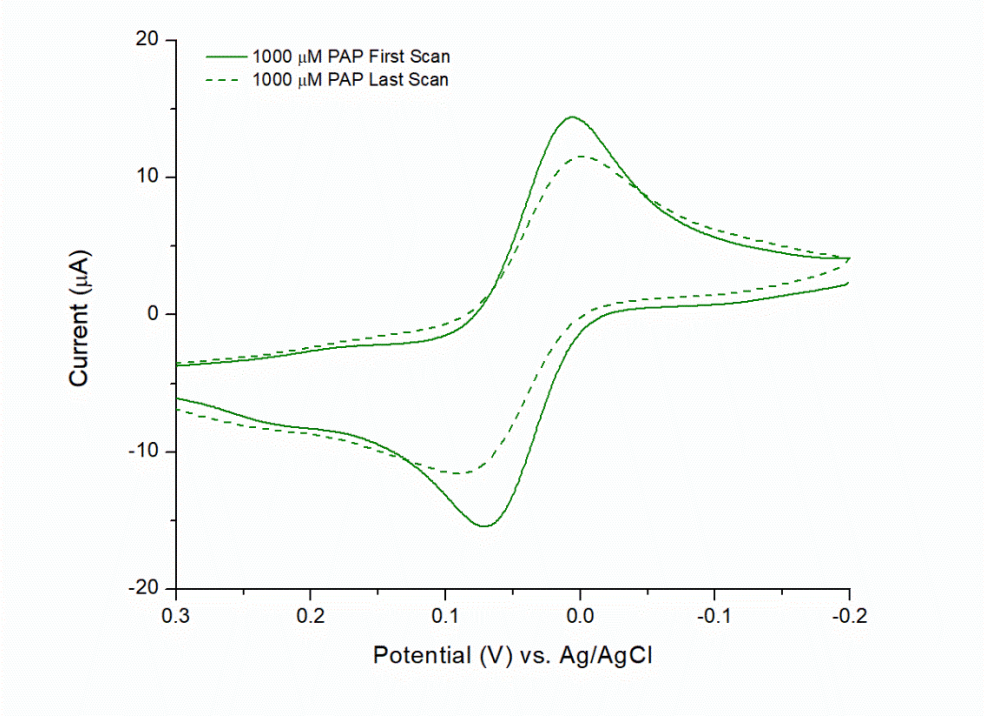

Figure 4.10. Overlays of 400 µM and 1000 µM PAP of the First and Last Scan of Cyclic Voltammograms. The increase in i_{pa} and i_{pc} reverses for these scans, with the last scan peaks below the first. However, the proportionality with concentration appears to hold still.

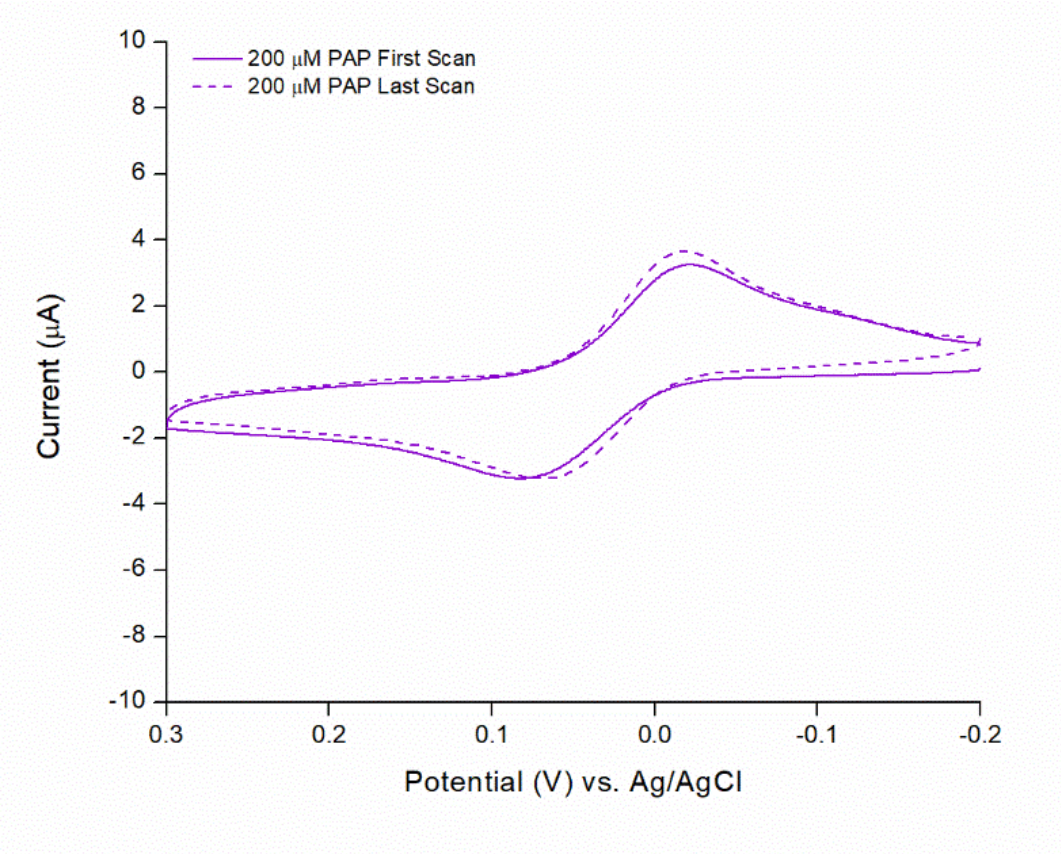

Figure 4.11. 200 µM PAP First and Last Scan Overlay. This concentration appeared to have the most minor change between the first and last scans.

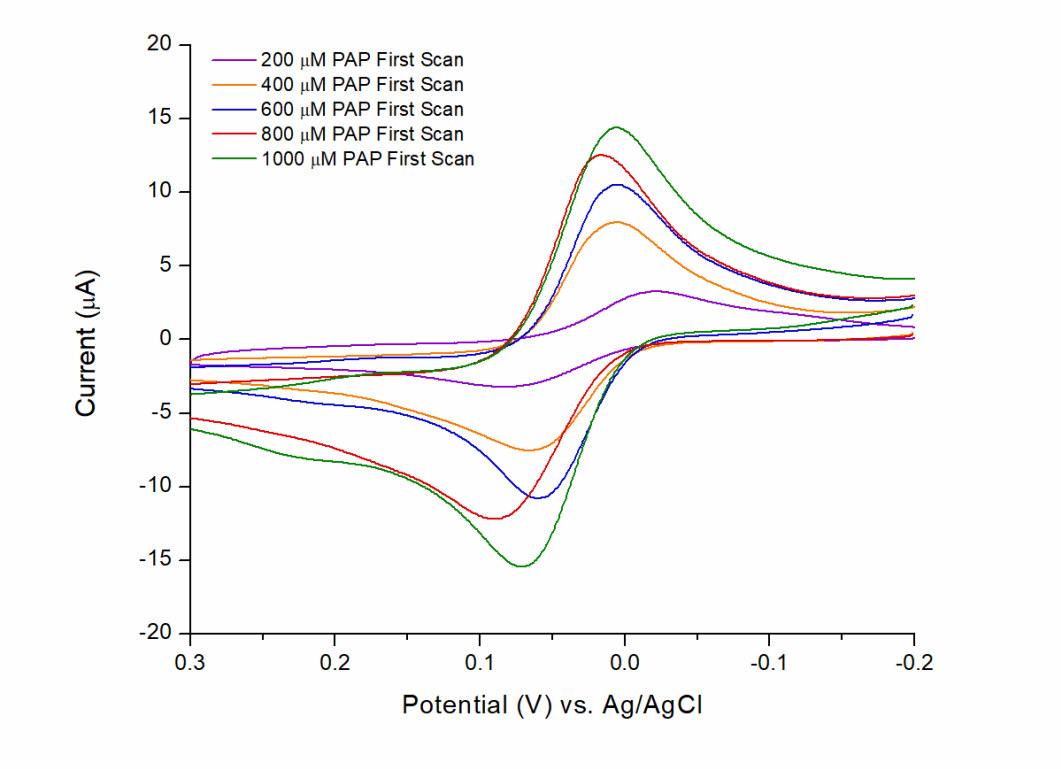

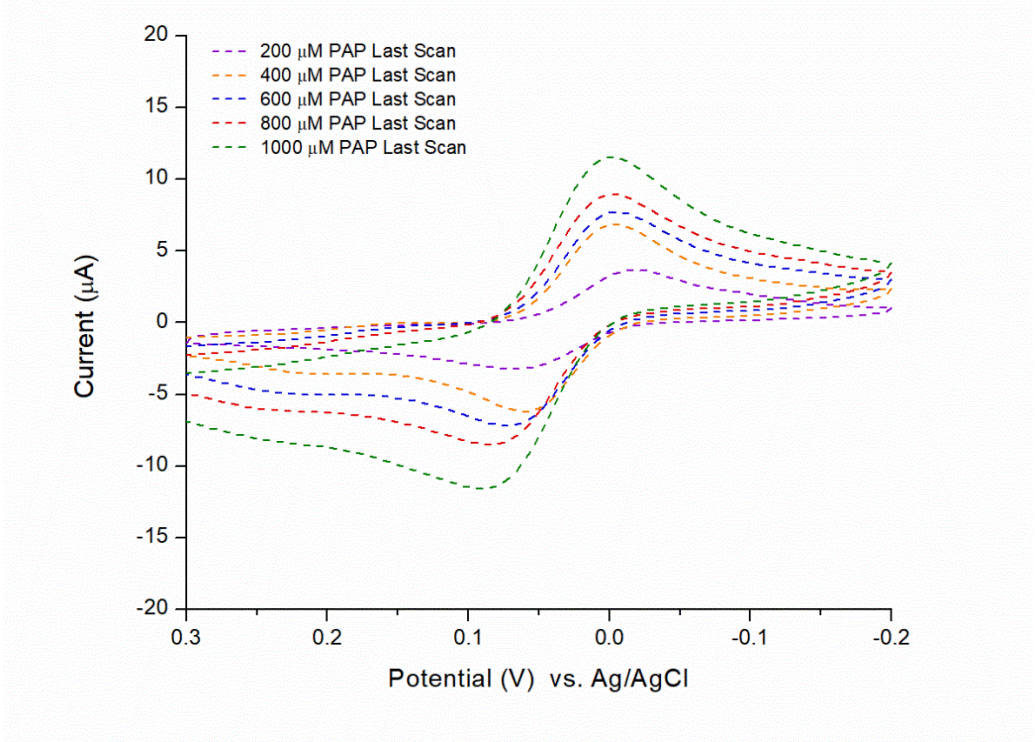

Figure 4.12. First Scan and Last Scan of 30 leg cyclic voltammogram cycle for multiple PAP concentrations. An additional oxidation peak grows in around +0.2 V (vs. Ag/AgCl) as the PAP concentration increases. The i_{pa} and i_{pc} decrease for all concentrations (except the 200 µM PAP).

The increase of peak current height for the lower concentration of PAP followed by the decrease of peak current height at the higher concentration of PAP indicates electro-polymerization and subsequent growth of PAP upon the electrode surface (figures 4.9 through 4.12). The lower concentrations current increase shows the monolayer formation, the smaller building blocks assisting in electron transfer, leading to increased current. This eventually leads to a plateau, and the film moves towards an extension. Due to the film's thickness, decreased electron transfer due to impedance will cause a decrease in current, as shown in the higher concentration CVs.

4.2.4. Conclusions & Future Outlooks

200 µM PAP shows the most promise for utilization within a sensor platform due to its most Nernstian behavior of all of the concentrations tested. Further testing should be performed to determine when polymerization occurs with this concentration PAP within the solution and does this hold with other types of electrodes. Possibility holds for a broader range of concentrations (that show typical CV behavior) with the combined use of a pulse pre-step for cleaning the electrode to remove any polymerization. Hopes for the sensor platform overall remain with optimization of all parameters.

5. STATIC SANDWICH ELECTROCHEMICAL IMMUNOASSAY (sECIA) FOR INTERLEUKIN-6

This chapter focuses on an electrochemical immunoassay to determine the blood concentration of Interleukin-6 (IL-6), a crucial biomarker for early sepsis detection. While the development of this diagnostic tool was originally for IL-6 and sepsis, the overall goal was to create a customizable sensing platform that could detect a variety of cytokines. Here the data regarding the preliminary testing, troubleshooting, and calibration curves are analyzed and discussed. A special thanks to MIDN 1/C Rochelle Gober, MIDN 2/C Isabella Penkwitz, and MIDN 2/C Andrew Mitchell, USN, for their contributions to this project during their summer internships. Additionally, my committee member Dr. Jonathan Schoenecker, M.D, Ph.D., and his group for bringing this collaboration to us. Also, thank you to Grace Buckey for her research contributions to this project during her rotation in our group.

5.1. Determination of layer weakness in ferrocene particle sandwich immunoassay.

5.1.1. Introduction

As previously discussed, IL-6 is a pro-inflammatory cytokine that assists in the body's natural immune response. IL-6 as a biomarker is used as a signal of tissue repair and can assist in the early determination of out-of-control immune responses. This makes it a viable candidate for a rapid, low-cost test that would allow for easy bedside diagnosis with clinicians and patients knowing when to seek hospitalization.

One example, with sepsis, the overwhelming immune response leads to organ failure.[43-44] Since sepsis appears symptomless or masquerades as other post-operative issues, early intervention is challenging. Still, it would also allow clinicians to treat the recovery rate is higher.

The IL-6 blood concentration is consistently between 0 – 2000 pg/mL as past 1000 pg/mL death is likely to occur in patients. As IL-6 concentrations indicate tissue repair, extremely low concentrations of IL-6 (below 100 pg/mL) are not clinically relevant. These are parameters that biosensors should take into account during the design process.

IL-6 Sensor

Chapter 4 discussed the different types of electrochemical IL-6 sensors in the literature. The overall terminology for electrochemical protein detection is electrochemical immunoassay or ECIA, with the three subcategories being direct ECIA (dECIA), indirect competitive (icECIA), and sandwich ECIA (sECIA). Here the sECIA will be focused on, since the work in this chapter focuses on the attempts to replicate and improve the sensor developed by Li *et al.*[74]

There is no current standard of care to readily enable this detection amongst patients since the current technology required to detect threshold concentration level of IL-6 requires a specific analytical tool known as an enzyme-linked immunosorbent assay (ELISA). For IL-6, this assay takes approximately 8-hours to complete, which is too long of a diagnostic for patients. Patients who necessitate this test either do not have access to an ELISA, or the time is this test is too long to justify its use as standard. The ideal solution would be an inexpensive, rapid test before discharge as a requirement to ensure that their inflammation levels showed no signs of illness.

This project aims to create an electrochemical sensor that will provide a linear range on the pg/mL concentration scale, easily customizable for various proteins. As such, an sECIA will be employed. This method explicitly uses a redox probe for detection. With the high sensitivity of electrochemical measurements, and modern electrodes shrinking the volume required for the electrochemical cell, the incubation time for an sECIA is significantly shorter than the traditional. This provides an advantage that can be used for time-sensitive medical diagnostics.

Described here is the development of such a diagnostic with redox-active porous nanoparticles adapted from Li *et al.* citation 13.[74] The sensors utilized in that work were a porous $CaCO_3$ nanoparticle-containing ferrocene and a porous polyelectrolyte outer layer serving to contain the redox probe while also acting as electron transport. A representation of this adaptation is shown in figure 5.1. The porosity of the particles and their distance from the electrode surface led to inconsistency during use—adherence of the base antibody film to the electrode surface eroded under repeated rinsing. A significant difference between layer impedance using EIS was not found between using EDC/NHS or Protein A.

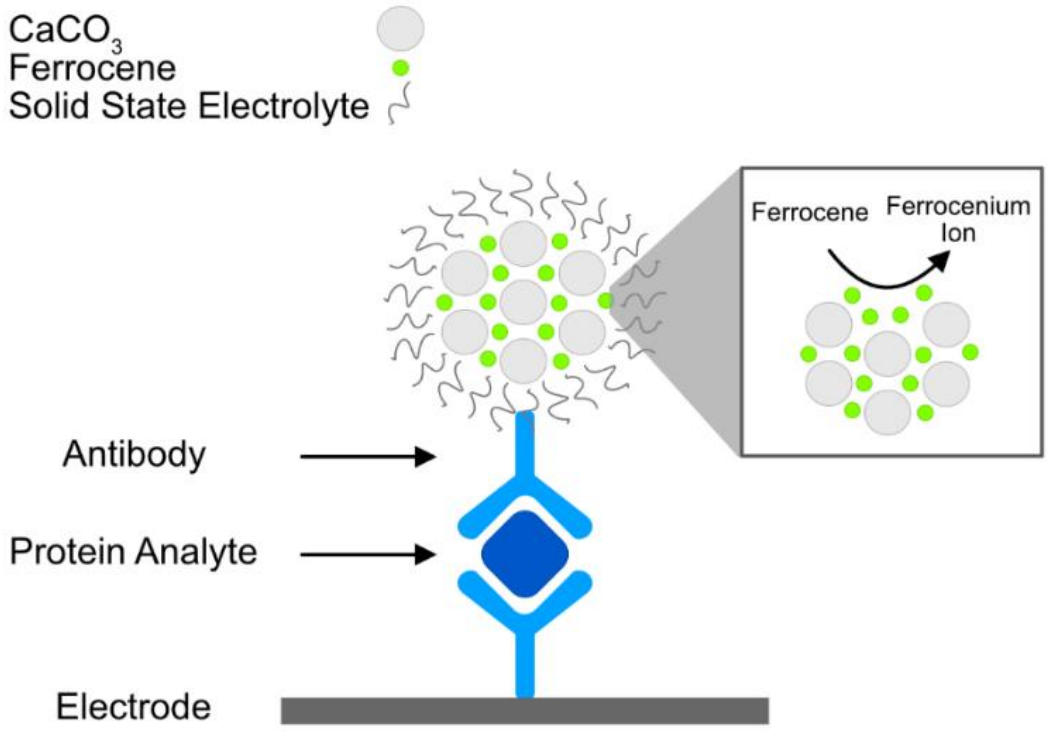

Figure 5.1. Electrochemical Immunoassay Representation. The calcium carbonate particles and the ferrocene were held in a solid-state electrolyte porous bag. The calcium carbonate particles assisted in keeping the ferrocene within the bag and allowing its diffusion to occur slowly. The rest of the sensor design is the traditional "antibody sandwich". The protein analyte is the antigen around which two antibodies bind. One antibody is stationary, attached to the electrode surface. The other is free, bound to the signal tag, and introduced later into the assay.

5.1.2. Materials and Methods

Chemicals and Materials

KCl (Certified ACS), 7.4 pH phosphate buffer solution (Certified ACS), sulfuric acid (Certified ACS plus, 98% concentration), and Na_2CO_3 (Certified ACS, anhydrous) were obtained from Fisher Scientific. The following chemicals were obtained from Sigma Aldrich: Poly(diallyldimethylammonium chloride) (PDDA; high molecular weight, 20% in water), Poly(acrylic acid) (PAA; average MW 100,000, 35% in water), ferrocene (IR and Elemental Analysis verified), 1-Ethyl-3-(3-dimethylaminopropyl)carbodiimide (EDC; commercial grade), N-Hydroxysuccinimide (NHS; 98%), bovine serum albumin (BSA; heat shock fraction, protease-free, pH 7, ≥98%) and Protein A (from *S. aureus,* soluble, essentially salt-free, lyophilized powder, extracellular). IL-6 Mouse anti-Human antibodies (monoclonal, Clone: 1936, unconjugated) and IL-6 Protein (Recombinant Human, Carrier Free) were obtained from R&D Systems. $CaCl_2$ (Ultra-Pure) was from Strem Chemicals. Ethanol (200 proof, USP specifications) was from Deacon. The Poly(styrene sulfonic acid) (PSS; MW 75,000) was from Beantown Chemical. DI water (18.2 MΩ) was used when necessary.

Ferrocene Particle Synthesis

Adapted from Li *et al.,* $CaCO_3$ nanoparticles were prepared by rapidly stirring with equal volumes (20 mL each) of 10 mM $CaCl_2$ and Na_2CO_3 solutions. The particles were then centrifuged, rinsed with DI water, and air-dried.[74]

To create the larger ferrocene-containing particles, an optimization resulted in 12.5 mg of ferrocene, 3 mg of polystyrene sulfonate (PSS), 3 mg of poly(diallyldimethylammoniumchloride) (PDDA), and 20 mg of $CaCO_3$ particles, dissolved in a 1:1 ratio of 200 proof ethanol and DI water. This solution was then stirred slowly and heated until 80-90% of the solution evaporated. The

metric (goal) was to evaporate as much solution as possible, and the solution was still thin enough that the stir bar was cleanly removed, leaving all solution behind. The solution was then placed under a nitrogen stream until dry (overnight). This combination created a porous particle (when resuspended in solution) that solubilized homogenously in water and allowed the ferrocene to be detected electrochemically. The dry powder was rinsed with 1:1 ethanol and DI water and redried using a nitrogen stream.

The final particles and the antibodies are bound together through electrostatic attraction. A 10 µg/mL solution of IL-6 Ab_2 solution in PBS pH 7.4 was prepared using lyophilized protein from R&D Systems. (Protein was obtained, and various concentrations and aliquots were made for multiple projects consumption). The particles were stirred with the antibody solution for 12 hours and then centrifuged (5000 rpm for 5 min). The particles were then resuspended in the buffer for a 1 mg/mL solution and stored at 4°C until use.

Preparation of Electrode Surface

Attachment of the antibody to the electrode occurred via a layer-by-layer deposition reported by Rusling *et al.*[75] using 10 µL of solution. The layering process began with PDDA (2 mg/mL in DI water) and poly(acrylic acid) (PAA) (2 mg/mL in DI water) together for 20 minutes, followed by 1-ethyl-3-(3-dimethylaminopropyl)carbodiimide hydrochloride (EDC) and N-hydroxysuccinimide (NHS) (400 mM/100 mM; freshly made in DI water) for 20 minutes. The addition of the IL-6 antibody followed this is added (100 µg/mL) for 20 minutes. Finally, 1% bovine serum albumin (BSA) was added to prevent non-specific binding. Each SPEs working electrode area was rinsed with water after each incubation. Areas that were plastic were dabbed dry to wick away excess moisture.

Administration of Assay

While a fully developed assay was not completed, a standard procedure to perform measurements with the prepared sensors was developed. A prepared sensor had 10 µL of the IL-6 protein solution drop cast onto the working electrode to incubate for 10 minutes, then rinsed with phosphate-buffered saline (PBS, pH 7.4). Then 20 µL of the ferrocene particle-bound antibodies (ferrocene tag) was drop cast to incubate for 10 minutes then rinsed with PBS. The sensor was connected to the potentiostat and placed into a solution of PBS/KCl, for square wave voltammetry (SWV) to be run.

During calibration curve attempts, the method of standard addition was used. The above procedure was followed, then after each SWV, an additional 10 µL sample was incubated on the sensor, followed by ferrocene tag, and another measurement was taken. This continued until 4-5 measurements had been made. Deviations to this procedure will be noted where appropriate.

Instrumentation and Characterization

All electrodes utilized are Pine Instruments carbon screen-printed electrodes (SPEs) with a 2-mm o.d., a Ag/AgCl reference electrode, and a carbon counter electrode. All electrochemical measurements were performed on CHI Potentiostat 620A and CHI Potentiostat 660. Carbon SPEs were acid cleaned according to the manufacturer's instructions.

SW Parameters

SWV was run with an initial potential of -0.2 V to a final potential of 0.4 V (vs. Ag/AgCl) with a 1×10^{-6}. Increment potential was 0.004 V, and amplitude was 0.025 V. Frequency was 15 Hz.

EIS Parameters

EIS was performed without a mediator at a potential of 0 V (vs. Ag/AgCl), and an amplitude of 0.005 V. Frequency was started at 1×10^{5} Hz and run to 1 Hz.

5.1.3. Results and Discussion

During the preparation of the sensor, trouble with the calibration signal led to the investigation of whether an additional step was required to add carboxylic acids to the surface of the electrode or if the natural carboxyl terminal groups on the surface of the carbon SPEs were sufficient for the EDC-NHS chemistry coupling of the antibody to the electrode. The theoretical structural differences between the two are shown in figure 5.2. Two sets of assays were run, one where only the EDC-NHS couple was used to create the antibody film, the second assay a carboxylic acid film on the electrode first using PDDA and PAA, followed by the EDC-NHS couple. The assay protocol was followed, as noted in the methods. The square wave voltammetry performed on the samples showed the effectiveness of the two preparations. The EDC-NHS prep did not show the peak (figure X) associated with ferrocene presence in the solution. The prep that included the PDDA/PAA shows a peak at +0.23 (vs. Ag/AgCl). This demonstrated that the acid-cleaned carbon SPE did not have enough carboxyl groups to make up the sensor base for this assay. Given the proprietary nature of the carbon ink used in the production of the SPEs, it is unclear exactly why acid cleaning did not produce more carboxylic acid groups for EDC-NHS addition. Further investigation into this matter could be performed with drop angle measurement to obtain a quantifiable hydrophilic vs. hydrophobic nature of the carbon electrode surface before and after acid cleaning.

Once the overall particles were synthesized, the sensors' design and antibody attachment needed to be verified. Two electrode preparation methods were compared to determine which was best for the given application. The first sensor utilized only carboxylic acids created on the carbon surface from the acid cleaning, and then those were used in the EDC/NHS coupling with the antibodies. The second sensor added two additional layers of PDDA and PAA before the

EDC/NHS to create a surface of carboxylic acids for the antibody coupling. In Figure 5.3, the two different scans are shown, after an excessive amount of protein (200,000 pg/mL, 20 µL drop cast) was added along with the ferrocene particle-tagged antibodies. They show that the PDDA/PAA created necessary carboxylic acids for the EDC/NHS coupling, resulting in a ferrocene signal shown in the second sensor.

Sensor stability was evaluated using a 500 pg/mL concentration and subsequent washes to determine how long the film would adhere and signal to the electrode surface. The results show in Figure 5.5 that after an initial rinse of one to two signal drops to near baseline current.

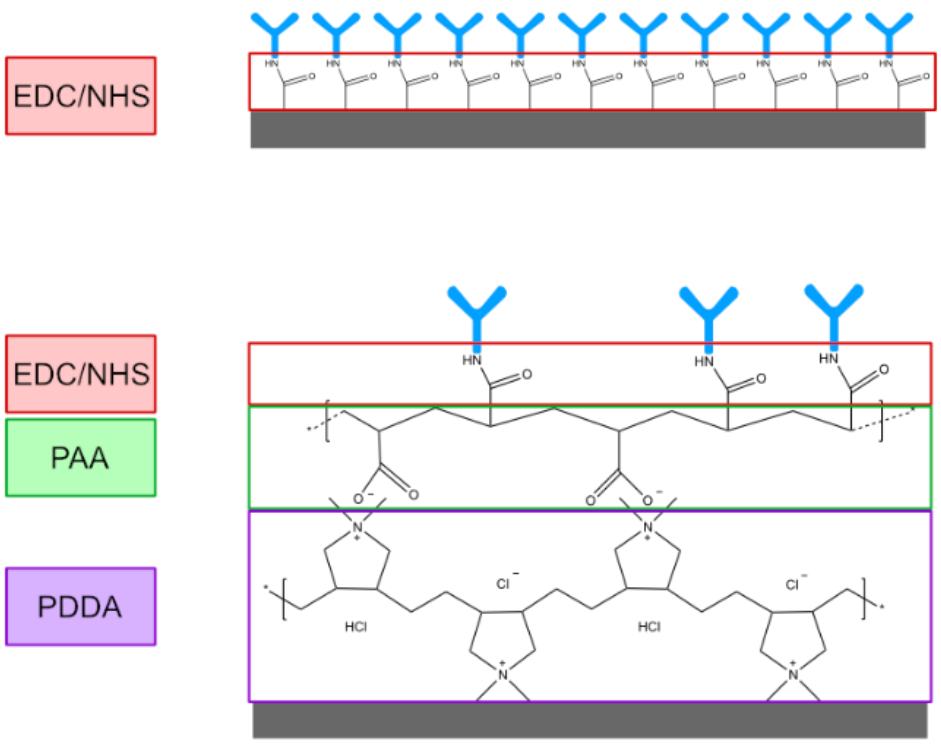

Figure 5.2. Structural Differences between EDC-NHS coupling and the addition of PDDA/PAA.

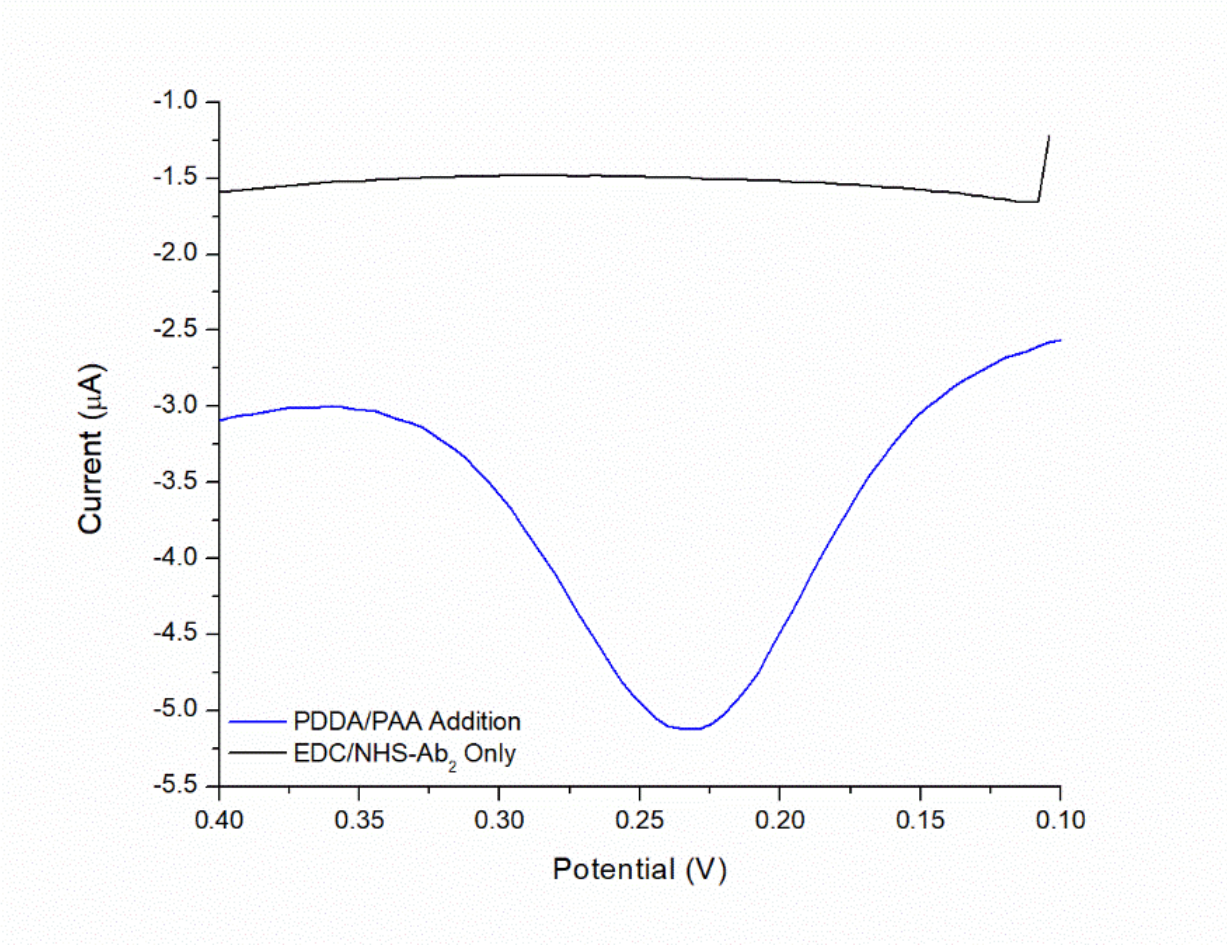

Figure 5.3. SWV of PDDA/PAA addition vs. EDC-NHS only Sensor preparation. Utilizing an acid clean on the carbon electrodes to generate carboxyl groups was unsuccessful. After performing the EDC-NHS couple, no ferrocene signal was detected in the square wave scan. Performing the same scan and conditions with the addition of PDDA/PAA to create a layer of carboxyl groups across the electrode surface generated the peak expected for ferrocene in aqueous solution vs. Ag/AgCl.

Concern over antigen removal to refresh the sensor surface versus damaging the underlying base sensor film led to the standard addition method to create calibration curves and eventual detection of samples. As shown in figure 5.4, the sensor was exposed to increasing concentrations of IL-6 protein, following the assay protocol. The peak current was recorded and is shown in the figure. There is an increasing linear trend, as expected. The current reaches a maximum of 750 pg/mL, with 1000 pg/mL and greater showing less current response with more concentration. This is a demonstration of the hook effect.[76] The hook effect is a known immunoassay response that occurs when either the tagged (free) antibody or antigen is in too high of a localized concentration resulting in conglomeration and diffusion away from the sensing apparatus, thus lowering the signal. This demonstrates a need to optimize the assay, the correct ratio of IL-6 concentration representing the blood concentration, and the tagged IL-6 antibodies for detection.

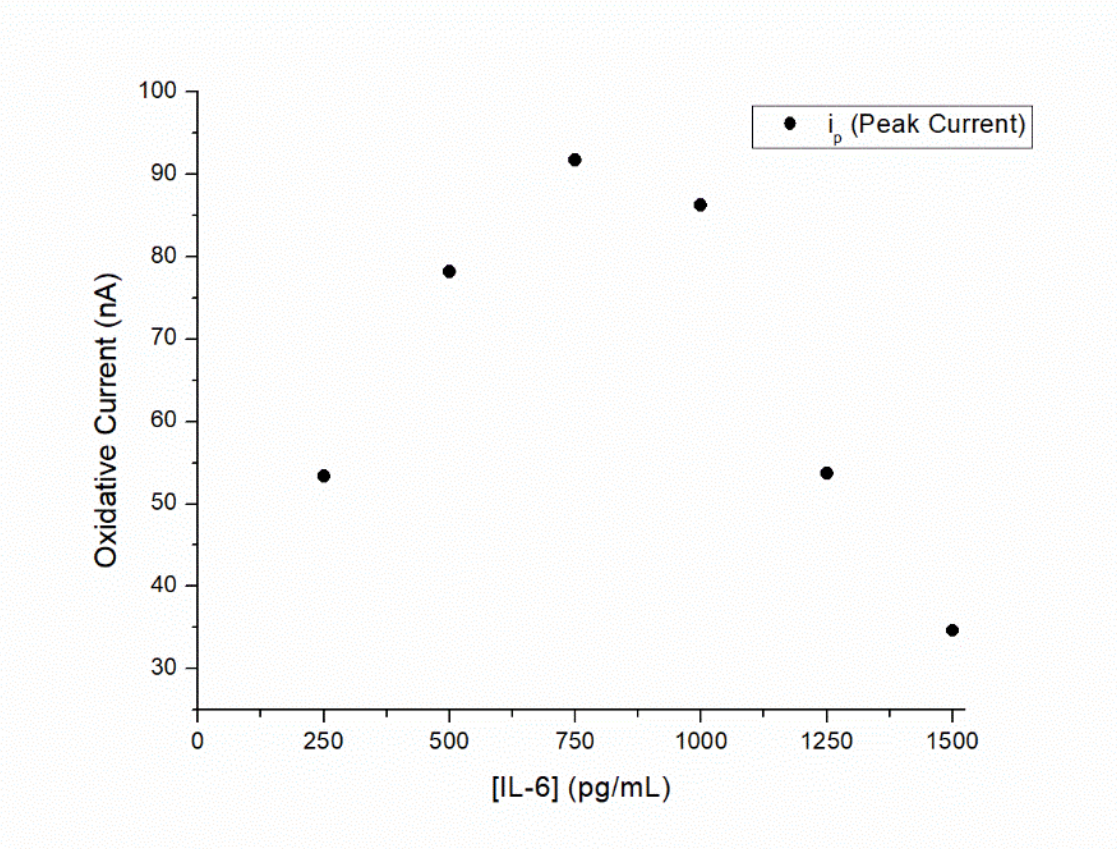

Figure 5.4. SWV peak plot of concentration vs. current. This attempt at a calibration curve, utilizing standard addition, shows the "hook effect," an interference issue in immunoassays that occurs when one of the immuno-reagents is too concentrated on the surface. This causes the unbinding/competing of the other immuno-reagents at the surface, leading to decreasing signal.

With a single sensor used for multiple runs during the standard addition method, film stability through multiple rinses was analyzed. A single sensor was exposed to the protocol with a 500 pg/mL IL-6 protein dose. After a single run, repeated rinsing occurred, with a run occurring after each. Loss of signal occurred after each subsequent rinse, with the signal becoming almost nothing by run 3 and back at baseline by run 4. Multiple points of contact for breakage are possible along the chain of this assay. Investigation of which point is the weakest will be pursued. However, it is possible that not necessarily one is particularly weak to repeated rinsing, more that the multiple points of contact increase the likelihood of breakage. The most likely place for film breakage is in the two electrostatic bond locations, between the PDDA and PAA in the electrode-antibody attachment and the antibody-tag attachment.

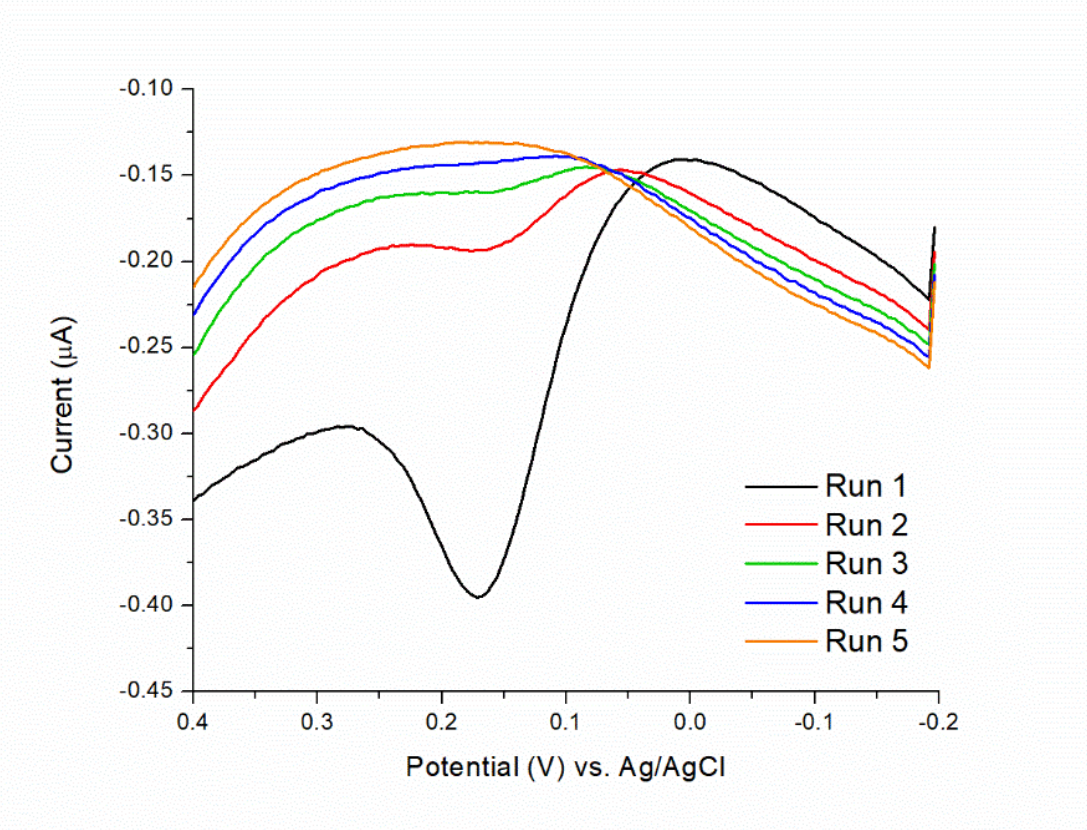

Figure 5.5. SWV peak plot of successive runs with rinsing in between. This series of scans showed an issue with film adherence on the electrode surface. The assay was performed with a 500 pg/mL concentration sample (run one) and was rinsed and scanned again (runs 2-5). The decrease with each scan demonstrates that some point of the film is weak and fails by simply rising with a pipette and buffer solution.

Using impedance techniques during film creation was used to determine which parts of the film were weak to determine which layers needed improvement. Additionally, two components were added to compare and contrast the current methodologies for improvement, sonication between steps and the substitution of protein A instead of the carboxylic acid/primary amine coupling through the PDDA/PAA/EDC chemistry. Protein A being one step instead of multiple steps was thought to minimize the error in these experiments and was thought to have stronger binding.77

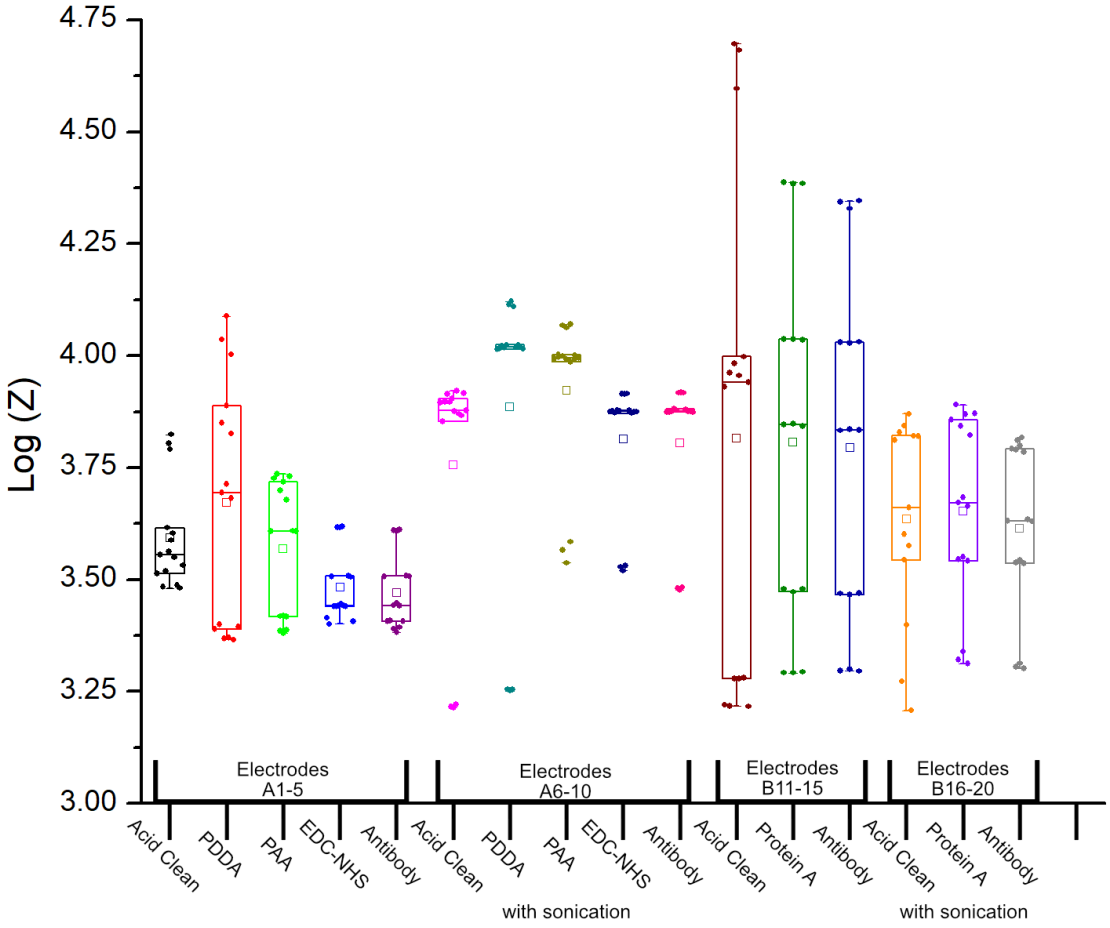

Figure 5.6. Impedance data of electrodes layer by layer. An investigation of each layer in building these sensors was performed with rinsing vs. sonication and comparing a carboxylic acid/amine polymer coupling vs. protein A. While the sonication improved the spread in the data measurements, there was no significant difference to show which layers were optimal for sensor development.

Each box within the graph comprises 15 measurements 5 electrodes measured in triplicate. The end EIS impedance was taken from each run to compose the data. The higher the log(Z), the larger the impedance of the sensor, meaning that the sensor would have a less likely chance of detecting the ferrocene tags needed to provide a calibrant or positive signal. The narrowing of the spread between the non-sonicated data versus sonicated data is expected. This is due to the effectiveness of sonication in rinsing the poorly surface-bound reactant or unreacted components compared to a wash bottle or pipette with a rinse solution. The extensive range of error in the protein A samples could be due to the age of protein A. Large amounts of bound protein could lead to high resistivity and no protein adherence.

Arguably the most interesting trend in this data is the lowered resistivity in the sensors as more layers are placed onto the electrode surface in the PDDA/EDC electrodes. While not statistically significant, the trend is not small and appears in both, potentially warrants follow-up investigation. This trend is also the opposite as one would expect. The PDDA/PAA layers are thin (compared to the biological ones) and contain multiple charged groups that should help lower the resistivity. The addition of the EDC/NHS falls in line with this hypothesis, and the data does reflect this. However, the addition of the antibody should spike the resistivity upwards due to its extensive, insulative nature. However, its addition does not raise resistivity and lowers it in several data points. This could potentially be that the number of antibodies attempting to bind to the surface of the electrode are unsuccessful and are instead ripping off previously placed portions of the film. This could be the point of film instability if the antibody concentration on the surface is “supersaturated” in a way. Even a few repeated washes would be able to force the film off.

5.1.4. Conclusions & Future Outlooks

The adaptation of the research from the previous authors did not lend itself to the new application. Altering the synthesis to limit the amount of polymer layer might assist with sensitivity in future experiments. The mechanism of action of this sensor is due to the diffusion of the ferrocene from within the solid electrolyte to out. This only allows the sensor to act statically and in no microfluidic capacity since its electrochemical sensing mechanism can only be dominated by diffusion and never convection. This constricts the sensor's applications, and its limited success in structural integrity does not provide enough reason to pursue this line of investigation further.

6. CONCLUSION & FUTURE DIRECTIONS

6.1. Summary

Electrochemical mediators provide a wide field of study but are of particular use to the study and development of biosensors. Since many biological molecules are insulators and not electrochemically active, it is important to develop analytical methods with a high degree of sensitivity and specificity. While other techniques are available, such as optical sensing, electrochemistry is extremely sensitive and low-cost, making it a strong contender as a platform for development.

Os-PVI shows strength in the electrochemical activity of redox polymers; however, when developing for a low-cost high throughput application such as biosensors, the utilization of osmium, a high-cost compound, is a concern. Another problem is the oxygen contamination that leaves the final polymer unsuitable for the designed application.

The PAP polymerization displays potentials issues with this compound in an electrochemical assay. However, the lack of change at the concentration of 200 µM shows that this concentration might limit the polymerization for the most prolonged period and make it a suitable candidate for specific assay applications.

No significant differences in the EIS data argue that the ferrocene particle design is an unreliable sensor platform. There appeared to be no one point in the layer-by-layer design that was particularly weak to wash steps.

6.2. Outlook

Os-PVI and f-Os-PVI are both simple to synthesize if using the proper equipment and synthetic procedures. If the correct need for their potentials arose, they would be well suited for

the task as reliable candidates. Additionally, since f-Os-PVI is both fluorescent and electrochemically active, it could potentially have electrogenerated-chemiluminescent applications.

Further investigation of PAP in the designed sensor apparatus and the determined sensor concentration should be explored. It is possible that issues concerning replication will not be an issue moving forward. It is also possible that using a pulse pre-step to clean the electrode between runs could also resolve the issues.

There is no recommendation regarding the ferrocene particles.

As evidenced by the projects described in this dissertation, more care needs to be taken during the investigation and publication of research pursuits. In Chapter 3, the difficulties in synthesizing the Os polymer could have been mitigated had previous researchers done their due diligence to fully characterize their materials and share those results via supplemental information. In all the target Os polymer literature, only one article shared a ^{1}H NMR, an essential and necessary characterization method for any organic or organometallic synthesis. This oversight could question whether previous papers made the target or whether they were using something else entirely. Additionally, Chapter 4 details how specific sensor platforms or techniques were claimed to be useful for applications well outside of their experimental parameters. Much of the literature regarding PAP takes place at either acidic/basic conditions or in non-aqueous environments yet claims to be useful for biological sensing purposes. These assertions were made with no data to support them, and their validity based on this work is in question. Chapter 5 displayed the attempts to replicate a sensor platform in the literature for IL-6 and attempts to salvage the platform when issues were occurring.

Hopefully, this dissertation has highlighted to the reader how one can communicate scientific data as a learning experience. Not every project will succeed; they are not supposed to. But even in failure, important information is obtained. Detailed and relevant conclusions must be made about what works and what directions to go next.

7. REFERENCES

1. The Nobel Prize in Chemistry 2019. https://www.nobelprize.org/prizes/chemistry/2019/press-release/ (accessed 2/20/2022).

2. Thurber, C. R.; Ahmad, Y. H.; Calhoun, M. C.; Al-Shenawa, A.; D'Souza, N.; Mohamed, A. M. A.; Golden, T. D., Metal Matrix Composite Coatings of Cupronickel Embedded with Nanoplatelets for Improved Corrosion Resistant Properties. *International Journal of Corrosion* **2018,** *2018*, 1-11.

3. Labs, F. Electroplating 101: How Metal Plating Works. https://formlabs.com/blog/electroplating-metal-plating/ (accessed 2/20/2022).

4. Lee, C.; Calhoun, M. C.; Dorriety, W.; Hanrahan, R.; Lancaster, F.; Calhoun, R. L., Screening of Novel Anti-Corrosion Coatings by Scanning Electrochemical Microscopy (SECM). *ECS Transactions* **2015,** *66* (30), 65-71.

5. Cliffel, D. E.; Calhoun, R. L., 25 Years of Scanning Electrochemical Microscopy. *Interface magazine* **2014,** *23* (2), 41-41.

6. Bard, A. J. F., L. R., *Electrochemical Methods: Fundamental and Applications*. 2nd Edition ed.; John Wiley & Sons Inc.: New Jersey, 2001.

7. Gizzie, E. A.; LeBlanc, G.; Jennings, G. K.; Cliffel, D. E., Electrochemical Preparation of Photosystem I–Polyaniline Composite Films for Biohybrid Solar Energy Conversion. *ACS Applied Materials & Interfaces* **2015,** *7* (18), 9328-9335.

8. Jules; Formisano, N.; Estrela, P.; Carrara, S.; Tkac, J., Electrochemical biosensors and nanobiosensors. *Essays in Biochemistry* **2016,** *60* (1), 69-80.

9. Pisoschi, A. M.; Pop, A.; Serban, A. I.; Fafaneata, C., Electrochemical methods for ascorbic acid determination. *Electrochimica Acta* **2014,** *121*, 443-460.

10. Zhu, C.; Ang, N. W. J.; Meyer, T. H.; Qiu, Y.; Ackermann, L., Organic Electrochemistry: Molecular Syntheses with Potential. *ACS Central Science* **2021,** *7* (3), 415-431.

11. Wang, P.; Jia, H., Chapter 20 - Power-Generation from Biorenewable Resources: Biocatalysis in Biofuel Cells. In *Bioprocessing for Value-Added Products from Renewable Resources*, Yang, S.-T., Ed. Elsevier: Amsterdam, 2007; pp 507-525.

12. Fultz, M. L.; Durst, R. A., Mediator compounds for the electrochemical study of biological redox systems: a compilation. *Analytica Chimica Acta* **1982,** *140* (1), 1-18.

13. Liang, W. Y., Excitons. *Physics Education* **1970,** *5* (4), 226-228.

14. Tamirat, A. G.; Guan, X.; Liu, J.; Luo, J.; Xia, Y., Redox mediators as charge agents for changing electrochemical reactions. *Chemical Society Reviews* **2020,** *49* (20), 7454-7478.

15. Brutinel, E. D.; Gralnick, J. A., Shuttling happens: soluble flavin mediators of extracellular electron transfer in Shewanella. *Appl Microbiol Biotechnol* **2012,** *93* (1), 41-8.

16. Liu, X.; Shi, L.; Gu, J.-D., Microbial electrocatalysis: Redox mediators responsible for extracellular electron transfer. *Biotechnology Advances* **2018,** *36* (7), 1815-1827.

17. Newman, J. D.; Setford, S. J., Enzymatic Biosensors. *Molecular Biotechnology* **2006,** *32* (3), 249-268.

18. Silveira, C. M.; Almeida, M. G., Small electron-transfer proteins as mediators in enzymatic electrochemical biosensors. *Analytical and Bioanalytical Chemistry* **2013,** *405* (11), 3619-3635.

19. Passantino, J. M.; Wolfe, K. D.; Simon, K. T.; Cliffel, D. E.; Jennings, G. K., Photosystem I Enhances the Efficiency of a Natural, Gel-Based Dye-Sensitized Solar Cell. *ACS Applied Bio Materials* **2020,** *3* (7), 4465-4473.

20. Choudhary, Y. S.; Jothi, L.; Nageswaran, G., Chapter 2 - Electrochemical Characterization. Elsevier Inc: 2017; pp 19-54.

21. Osteryoung, J. G.; Osteryoung, R. A., Square Wave Voltammetry. *Analytical Chemistry* **1985,** *57* (1), 101A-110A.

22. Instruments, G. Chronoamperometry Purpose. https://www.gamry.com/Framework%20Help/HTML5%20-%20Tripane%20-%20Audience%20A/Content/PE/Experimental_Techniques/Chronoamperometry/Purpose.htm (accessed 2/21/2022).

23. Calhoun, M. C.; Stachurski, C. D.; Winn, S. L.; Gizzie, E. A.; Daniel, A. W.; Schley, N. D.; Cliffel, D. E., Trace Oxygen Affects Osmium Redox Polymer Synthesis for Wired Enzymatic Biosensors. *Journal of The Electrochemical Society* **2022,** *169* (1), 016506.

24. Casado, N.; Hernández, G.; Sardon, H.; Mecerreyes, D., Current trends in redox polymers for energy and medicine. *Progress in polymer science* **2016,** *52*, 107-135.

25. Melow, S. L.; Miller, D. R.; Gizzie, E. A.; Cliffel, D. E., A low-interference, high-resolution multianalyte electrochemical biosensor. *Analytical methods* **2020,** *12* (31), 3873-3882.

26. Ohara, T. J.; Rajagopalan, R.; Heller, A., Glucose electrodes based on cross-linked [Os(bpy)2Cl]+/2+ complexed poly(1-vinylimidazole) films. *Anal Chem* **1993,** *65* (23), 3512-7.

27. Ohara, T. J.; Rajagopalan, R.; Heller, A., "Wired" enzyme electrodes for amperometric determination of glucose or lactate in the presence of interfering substances. *Anal Chem* **1994,** *66* (15), 2451-7.

28. Kurbanoglu, S.; Zafar, M. N.; Tasca, F.; Aslam, I.; Spadiut, O.; Leech, D.; Haltrich, D.; Gorton, L., Amperometric Flow Injection Analysis of Glucose and Galactose Based on

Engineered Pyranose 2-Oxidases and Osmium Polymers for Biosensor Applications. *Electroanalysis (New York, N.Y.)* **2018,** *30* (7), 1496-1504.

29. Osadebe, I.; Conghaile, P. Ó.; Kavanagh, P.; Leech, D., Glucose oxidation by osmium redox polymer mediated enzyme electrodes operating at low potential and in oxygen, for application to enzymatic fuel cells. *Electrochimica acta* **2015,** *182*, 320-326.

30. Kober, E. M.; Caspar, J. V.; Sullivan, B. P.; Meyer, T. J., Synthetic routes to new polypyridyl complexes of osmium(II). *Inorganic Chemistry* **1988,** *27* (25), 4587-4598.

31. D. A. Buckingham, F. P. D., H. A. Goodwin, and A. M. Sargeson, Mono- and Bis-(2,2'-Bipyridine) and (1,10-phenanthroline)
Chelates of Ruthenium and Osmium: IV. Bis Chelates of Bivalent and Tetravalent Osmium. *Australian Journal of Chemistry* **1963,** *17*, 325-36.

32. Andryj, B. The Schlenk Line Survival Guide. https://schlenklinesurvivalguide.com/.

33. Haddox, R. M.; Finklea, H. O., Proton-Coupled Electron Transfer of an Osmium Aquo Complex on a Self-Assembled Monolayer on Gold. *The Journal of Physical Chemistry B* **2004,** *108* (5), 1694-1700.

34. Madhiri, N.; Finklea, H. O., Potential-, pH-, and isotope-dependence of proton-coupled electron transfer of an osmium aquo complex attached to an electrode. *Langmuir* **2006,** *22* (25), 10643-51.

35. Mamo, A.; Aureliano, A.; Recca, A., Asymmetric ruthenium(II) and osmium(II) complexes with new bidentate polyquinoline ligands. Synthesis and NMR characterization. *Molecules* **2010,** *15* (3), 1324-39.

36. Togano, T.; Nagao, N.; Tsuchida, M.; Kumakura, H.; Hisamatsu, K.; Howell, F. S.; Mukaida, M., One-pot and selective synthesis of a series of [RuCl6−2nLn] (L=bidentate ligand,

n=0−3) types of complexes with polypyridyl ligands; another example of the synthetic utility of 'ruthenium-blue' solution. *Inorganica Chimica Acta* **1992,** *195* (2), 221-225.

37. Pekel, N.; Rzaev, Z. M. O.; Güven, O., Synthesis and Characterization of Poly(N-vinylimidazole-co-acrylonitrile) and Determination of Monomer Reactivity Ratios. *Macromolecular Chemistry and Physics* **2004,** *205* (8), 1088-1095.

38. Graham Solomons, T. W.; Fryhle, C. B.; Snyder, S. A., *Organic Chemistry 11E*. 11 ed.; John Wiley & Sons: Nashville, TN, 2012.

39. Gao, Z.; Binyamin, G.; Kim, H. H.; Barton, S. C.; Zhang, Y.; Heller, A., Electrodeposition of redox polymers and co-electrodeposition of enzymes by coordinative crosslinking. *Angew Chem Int Ed Engl* **2002,** *41* (5), 810-3.

40. Gibson, B. H. Y.; Wollenman, C. C.; Moore-Lotridge, S. N.; Keller, P. R.; Summitt, J. B.; Revenko, A. R.; Flick, M. J.; Blackwell, T. S.; Schoenecker, J. G., Plasmin drives burn-induced systemic inflammatory response syndrome. *JCI Insight* **2021,** *6* (23).

41. Baker, C. E.; Moore-Lotridge, S. N.; Hysong, A. A.; Posey, S. L.; Robinette, J. P.; Blum, D. M.; Benvenuti, M. A.; Cole, H. A.; Egawa, S.; Okawa, A.; Saito, M.; McCarthy, J. R.; Nyman, J. S.; Yuasa, M.; Schoenecker, J. G., Bone Fracture Acute Phase Response—A Unifying Theory of Fracture Repair: Clinical and Scientific Implications. *Clinical Reviews in Bone and Mineral Metabolism* **2018,** *16* (4), 142-158.

42. Vatansever, H. S.; Becer, E., Relationship between IL-6 and COVID-19: to be considered during treatment. *Future Virology* **2020,** *15* (12), 817-822.

43. Foex, B. A., Systemic responses to trauma. *Br Med Bull* **1999,** *55* (4), 726-43.

44. MedlinePlus Sepsis https://medlineplus.gov/sepsis.html.

45. Khan, M. A.; Mujahid, M., Recent Advances in Electrochemical and Optical Biosensors Designed for Detection of Interleukin 6. *Sensors* **2020,** *20* (3), 646.

46. Tertiş, M.; Ciui, B.; Suciu, M.; Săndulescu, R.; Cristea, C., Label-free electrochemical aptasensor based on gold and polypyrrole nanoparticles for interleukin 6 detection. *Electrochimica Acta* **2017,** *258*, 1208-1218.

47. Chen, H.; Choo, T. K.; Huang, J.; Wang, Y.; Liu, Y.; Platt, M.; Palaniappan, A.; Liedberg, B.; Tok, A. I. Y., Label-free electronic detection of interleukin-6 using horizontally aligned carbon nanotubes. *Materials & Design* **2016,** *90*, 852-857.

48. Yang, T.; Wang, S.; Jin, H.; Bao, W.; Huang, S.; Wang, J., An electrochemical impedance sensor for the label-free ultrasensitive detection of interleukin-6 antigen. *Sensors and Actuators B: Chemical* **2013,** *178*, 310-315.

49. Lou, Y.; He, T.; Jiang, F.; Shi, J.-J.; Zhu, J.-J., A competitive electrochemical immunosensor for the detection of human interleukin-6 based on the electrically heated carbon electrode and silver nanoparticles functionalized labels. *Talanta* **2014,** *122*, 135-139.

50. Information, N. C. f. B. ALPL alkaline phosphatase, biomineralization associated [Homo sapiens (human)] Gene ID: 249. https://www.ncbi.nlm.nih.gov/gene/249 (accessed 2/21/2022).

51. Lowe D, S. T., John S. Alkaline Phosphatase. https://www.ncbi.nlm.nih.gov/books/NBK459201/.

52. Mobley, D. M.; Chengappa, M. M.; Kadel, W. L.; Stuart, J. G., Effect of pH, temperature and media on acid and alkaline phosphatase activity in "clinical" and "nonclinical" isolates of Bordetella bronchiseptica. *Can J Comp Med* **1984,** *48* (2), 175-178.

53. Tu, Z.; Zhang, J.; Yang, G.; He, G., Characterization of alkaline phosphatase labeled UidA(Gus) probe and its application in testing of transgenic tritordeum. *Molecular Biology Reports* **2011,** *38* (6), 3629-3634.

54. Rodig, S. J., Counterstaining, Mounting, and Photographing Stained Cells. *Cold Spring Harbor Protocols* **2019,** *2019* (4), pdb.prot099770.

55. Wright, A. C.; Miceli, G. A.; Landry, W. L.; Christy, J. B.; Watkins, W. D.; Morris, J. G., Rapid identification of Vibrio vulnificus on nonselective media with an alkaline phosphatase-labeled oligonucleotide probe. *Applied and Environmental Microbiology* **1993,** *59* (2), 541-546.

56. Halsall, H. H. W., Elecrochemical immunoassay: an ultrasensitive method. *Journal of International Federation of Clinical Chemistry* **1990,** *2* (4), 179-89.

57. Xu, Y.; Halsall, H. B.; Heineman, W. R., Solid-phase electrochemical enzyme immunoassay with attomole detection limit by flow injection analysis. *Journal of Pharmaceutical and Biomedical Analysis* **1989,** *7* (12), 1301-1311.

58. Vargas, E.; Povedano, E.; Krishnan, S.; Teymourian, H.; Tehrani, F.; Campuzano, S.; Dassau, E.; Wang, J., Simultaneous cortisol/insulin microchip detection using dual enzyme tagging. *Biosensors and Bioelectronics* **2020**, 112512.

59. Weston, M. C.; Nash, C. K.; Fritsch, I., Redox-magnetohydrodynamic microfluidics without channels and compatible with electrochemical detection under immunoassay conditions. *Anal Chem* **2010,** *82* (17), 7068-72.

60. Tomoda, A.; Yamaguchi, J.; Kojima, H.; Amemiya, H.; Yoneyama, Y., Mechanism of o -aminophenol metabolism in human erythrocytes. *FEBS Letters* **1986,** *196* (1), 44-48.

61. Yang, X.; Kulkarni, A. P., Lipoxygenase-mediated biotransformation of p-aminophenol in the presence of glutathione: possible conjugate formation. *Toxicology Letters* **2000,** *111* (3), 253-261.

62. Yoshida, R.; Oikawa, S.; Ogawa, Y.; Miyakoshi, Y.; Ooida, M.; Asanuma, K.; Shimizu, H., Mutagenicity of p-aminophenol in E. coli WP2uvrA/pKM101 and its relevance to oxidative DNA damage. *Mutation Research/Genetic Toxicology and Environmental Mutagenesis* **1998,** *415* (1), 139-150.

63. Schwarz, J.; Oelßner, W.; Kaden, H.; Schumer, F.; Hennig, H., Voltammetric and spectroelectrochemical studies on 4-aminophenol at gold electrodes in aqueous and organic media. *Electrochimica Acta* **2003,** *48* (17), 2479-2486.

64. Yin, H.; Ma, Q.; Zhou, Y.; Ai, S.; Zhu, L., Electrochemical behavior and voltammetric determination of 4-aminophenol based on graphene–chitosan composite film modified glassy carbon electrode. *Electrochimica Acta* **2010,** *55* (23), 7102-7108.

65. Wang, J.; Jin, B.; Cheng, L., Investigation on redox mechanism of p-aminophenol in non-aqueous media by FT-IR spectroelectrochemistry. *Electrochimica Acta* **2013,** *91*, 152-157.

66. M.D., J. L. L. I. Overview of Acid-Base Balance. https://www.merckmanuals.com/home/hormonal-and-metabolic-disorders/acid-base-balance/overview-of-acid-base-balance.

67. Lindsay M. Biga, S. D., Amy Harwell, Robin Hopkins, Joel Kaufmann, Mike LeMaster, Philip Matern, Katie Morrison-Graham, Devon Quick & Jon Runyeon, *Anatomy and Physiology: 26.5 Disorders of Acid-Base Balance*. OpenStax; Pressbooks; Oregon State University.

68. Burger MK, S. D. Metabolic Acidosis. https://www.ncbi.nlm.nih.gov/books/NBK482146/ (accessed 2/21/2022).

69. E. Hopkins, T. S., and S. Sharma Physiology, Acid Base Balance. https://www.ncbi.nlm.nih.gov/books/NBK507807/.

70. Nematollahi, D.; Shayani-Jam, H.; Alimoradi, M.; Niroomand, S., Electrochemical oxidation of acetaminophen in aqueous solutions: Kinetic evaluation of hydrolysis, hydroxylation and dimerization processes. *Electrochimica Acta* **2009,** *54* (28), 7407-7415.

71. Beiginejad, H.; Nematollahi, D.; Varmaghani, F., Electrochemical Oxidation of Some Aminophenols in Various pHs. *Journal of The Electrochemical Society* **2012,** *160* (1), H41-H46.

72. Bannanakere N. Chandrashekar, B. E. K. S., Mundargi Pandurangachar, Tammanekar V. Sathisha and Bailure S. Sherigara, Electrochemical Investigation of 4-Aminophenol at CTAB Modified Carbon Paste Electrode: A Cyclic Voltammetric Technique. *Analytical and Bioanalytical Electrochemistry* **2011,** *3* (3), 227-232.

73. Taj, S.; Ahmed, M. F.; Sankarapapavinasam, S., Poly(para-aminophenol): a new soluble, electroactive conducting polymer. *Journal of Electroanalytical Chemistry* **1992,** *338* (1), 347-352.

74. Li, T.; Yang, M., Electrochemical sensor utilizing ferrocene loaded porous polyelectrolyte nanoparticles as label for the detection of protein biomarker IL-6. *Sensors and Actuators B: Chemical* **2011,** *158* (1), 361-365.

75. Kadimisetty, K.; Mosa, I. M.; Malla, S.; Satterwhite-Warden, J. E.; Kuhns, T. M.; Faria, R. C.; Lee, N. H.; Rusling, J. F., 3D-printed supercapacitor-powered electrochemiluminescent protein immunoarray. *Biosens Bioelectron* **2016,** *77*, 188-93.

76. Schiettecatte, J.; Anckaert, E.; Smitz, J., Interferences in Immunoassays. InTech: 2012.

77. Scheller, F. W.; Bistolas, N.; Liu, S.; Jänchen, M.; Katterle, M.; Wollenberger, U., Thirty years of haemoglobin electrochemistry. *Advances in Colloid and Interface Science* **2005,** *116* (1), 111-120.

78. Ye, J.; Baldwin, R. P., Catalytic reduction of myoglobin and hemoglobin at chemically modified electrodes containing methylene blue. *Analytical Chemistry* **1988,** *60* (20), 2263-2268.

8. METHYLENE BLUE THIN FILM HEMOGLOBIN SENSOR FOR THE DETERMINATION OF REDOX STATE REPRODUCIBILITY

This appendix provides sample analysis as part of a larger manuscript investigating the differences between commercial and freshly isolated human hemoglobin samples. My contribution looked at the oxidation states of the hemoglobin and the electrocatalytic activity of the samples provided. My knowledge of the sample preparation (specifically regarding the isolation of the human hemoglobin) was limited for scientific blindness. The results will be included in a manuscript for publication, with my results assisting in a broader conclusion. That manuscript will not be in publication at the time of submission of this dissertation but might be at the time of embargo release. Aqeela Afzal is the primary author of the publication in reference. I would like to thank her and Kelly Richardson for their assistance in this work and for including me in this project. Thank you to Aqeela Afzal and her funding partners for providing samples and reagents. Thank you to Kelly Richardson and Dr. David Wright for additional reagents.

8.1. Methylene Blue Thin Film Sensor Ineffective Due to Possible Additives in Commercial Hemoglobin Samples

8.1.1. Introduction

The homogenous redox couple of the reduced form of hemoglobin (ferrous hemoglobin) and the oxidized form of hemoglobin (ferric hemoglobin) is estimated to be -70 mV vs. SCE (saturated calomel electrode). However, the experimentation estimates that different portions of the protein (alpha helices vs. beta chains) might have different potentials.[77]

Direct heterogeneous electron transfer with ferric and ferrous hemoglobin has been attempted over several decades. Isolation of the hemoglobin is required as other proteins in solution will shift potentials and decrease peak heights if left in solution. Overall, bare electrodes

are not able to properly characterize hemoglobin since the protein's metal center is not easily accessible to the electrode surface.[77]

There are four popular solutions for modifying the electrode surface with indirect heterogeneous electron transfer to enable detection: mediators, nanoparticles, polymers, and lipids. Compounds such as riboflavin, poly(Nile blue), and methylene blue are traditional electrochemical mediators used to facilitate the electron transfer from hemoglobin to the electrode surface by acting as an electron shuttle. These compounds can interface more easily with the protein, access the metal center, and pass the electron onto the electrode for signal readout. Nanoparticle-modified or colloidal nanoparticle electrodes act in the same manner as mediator electrodes, wherein the nanoparticles on the surface provide easier access to the metal center of the hemoglobin. Polymer and lipid-modified electrodes create films that incorporate hemoglobin within them, attempting to mediate and mimic a functioning environment for hemoglobin to enhance the electron transfer rates. These methodologies are used in isolation or combined to either study hemoglobin redox chemistry or for biosensor creation.[77]

Afzal *et al.* (in preparation) found during the treatment of various human cells with commercial hemoglobin of both oxidation states that dense aggregates of unknown composition would form, destroying the cellular environment. Further investigation found this occurrence common and likely results from the stabilizing additives used with hemoglobin for commercial use. A novel method was developed to convert freshly isolated human hemoglobin from one redox state to another to prevent using chemical redox agents requiring further purification. Cyclic Voltammetry was utilized as an analytical method to characterize the four samples, freshly isolated ferrous (Hb2+) and ferric (Hb3+) and commercial Hb2+ and 3+. Discussion of Afzal *et al.* will be limited unless required for my portion of the work.

8.1.2. Materials and Methods

Chemicals and Sample Preparation

Ferric (Hb^{3+}) Hemoglobin was purchased from Cell Sciences (Newburyport, MA) or Sigma Aldrich (St Louis, MO). A minimum of three different lot numbers were tested for each commercial source of ferric hemoglobin. Deionized water was purchased from Millipore Sigma (Burlington, MA). Additional chemicals were purchased from Thermo Fisher Scientific unless otherwise stated.

The author did not perform the ferric (Hb3+) to Ferrous (Hb2+) Hemoglobin transition and was isolated from procedure knowledge to eliminate potential bias.

Hemoglobin samples were either isolated from human blood or purchased from a commercial source. These were isolated and purified, and portions were converted from the ferric (Hb^{3+}) form into the ferrous (Hb^{2+}) form. These four hemoglobin samples were provided for testing. They were diluted in a 2mM pH 7.4 phosphate-buffered solution and 120 mM KCl to a final concentration of 10 µM.

Electrochemical Set Up

Electrochemical measurements were obtained using a 900D Potentiostat (CH Instruments, Inc. Austin, TX), a 2mm diameter Au working electrode, a Ag/AgCl (1M) reference electrode, and a 0.5mm diameter Pt counter (99.95% platinum wire and mesh). The working electrode was polished using Bruker diamond paste (0.25 and 0.10 µm) and Alumina powder (0.05 µm).

Methylene Blue Film

A methylene blue film was formed on the electrode surface to provide a platform for catalytically mediated electron transfer. This method is often used to assist in the electrochemical analysis of proteins whose metal centers are not easily accessible to the electrode surface.[78] To add the methylene blue film to the working electrode, it was held for 60 seconds within a stirring

solution of 0.01% (w/v) aqueous solution of methylene blue in 0.10 M pH 5.3 phosphate buffer rinsed thoroughly with deionized water.[78]

Cyclic Voltammetry

Each cyclic voltammogram (CV) was performed as identically as possible for each sample depending upon the redox state of the hemoglobin. Freshly Isolated and commercial ferrous hemoglobin samples were run from -0.5 V to 0.5 V and back. Freshly isolated and commercial ferric hemoglobin were run from 0.5 V to -0.5 V and back. All samples were run at a scan rate of 0.1 V/sec with a sensitivity of 1×10^{-6}. Oxygen was unnoticed during the scans.

8.1.3. Results and Discussion

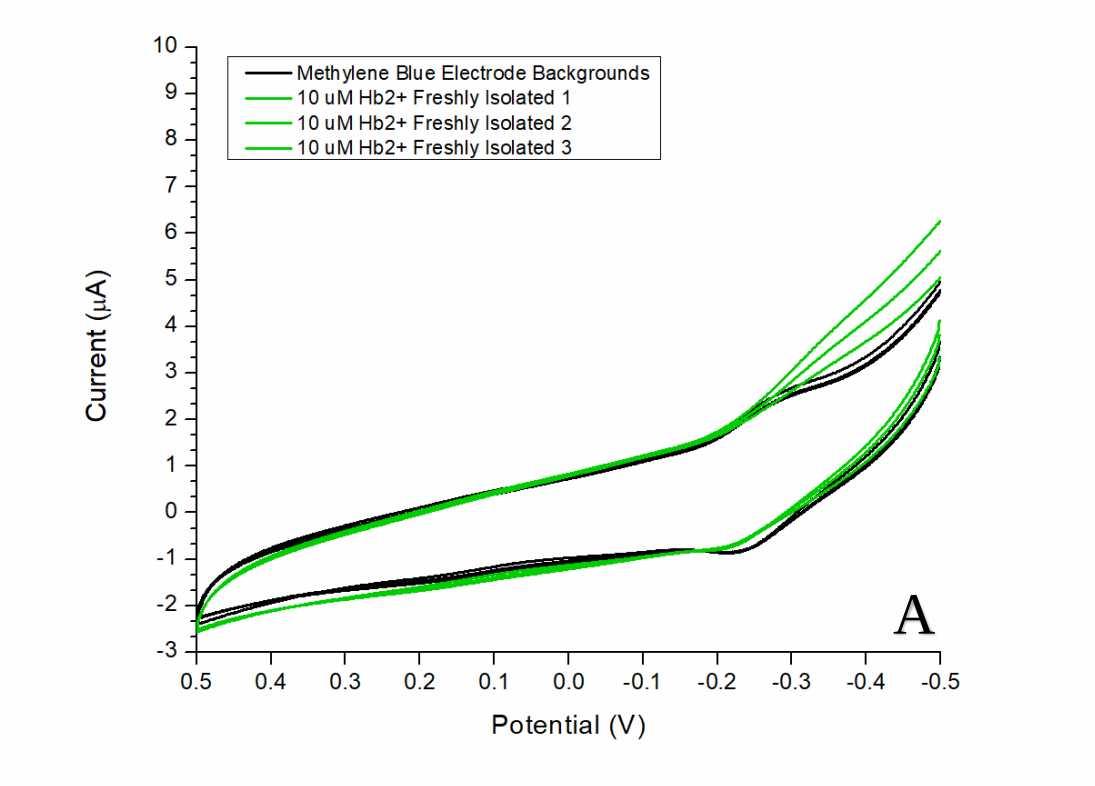

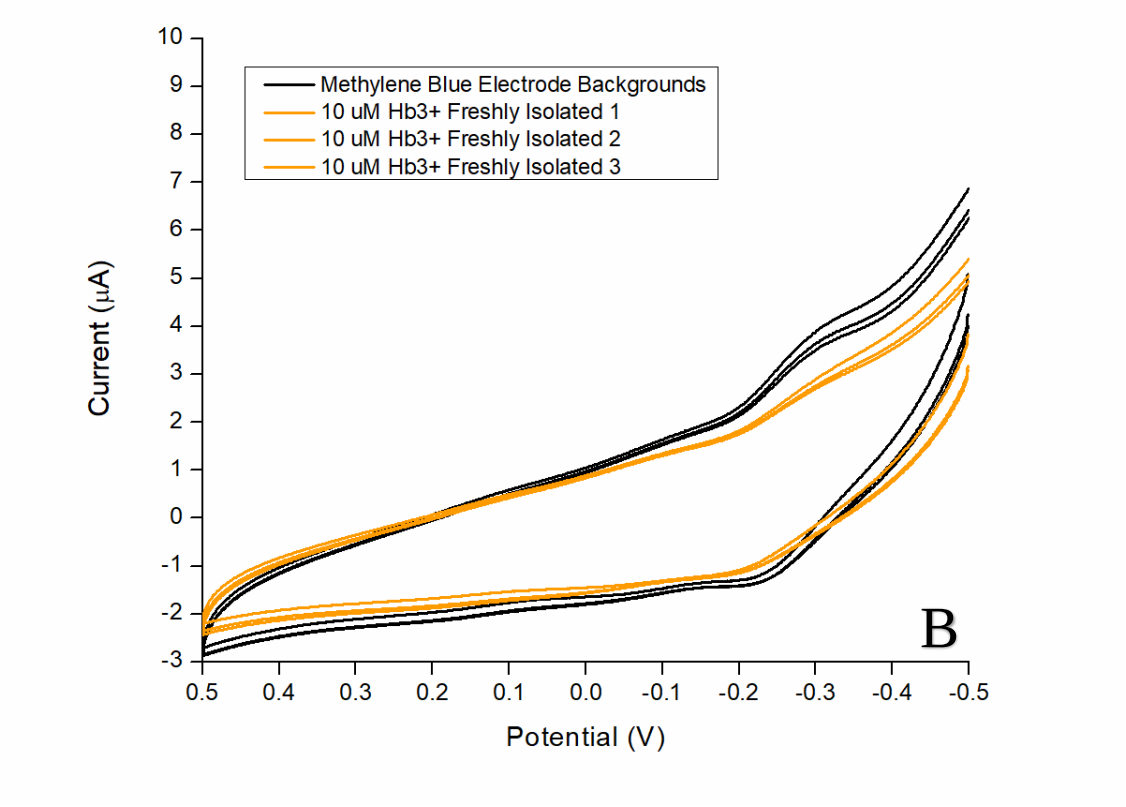
Methylene Blue Electrode Backgrounds
10 uM Hb3+ Freshly Isolated 1
10 uM Hb3+ Freshly Isolated 2
10 uM Hb3+ Freshly Isolated 3
Current (μA)
Potential (V)
B

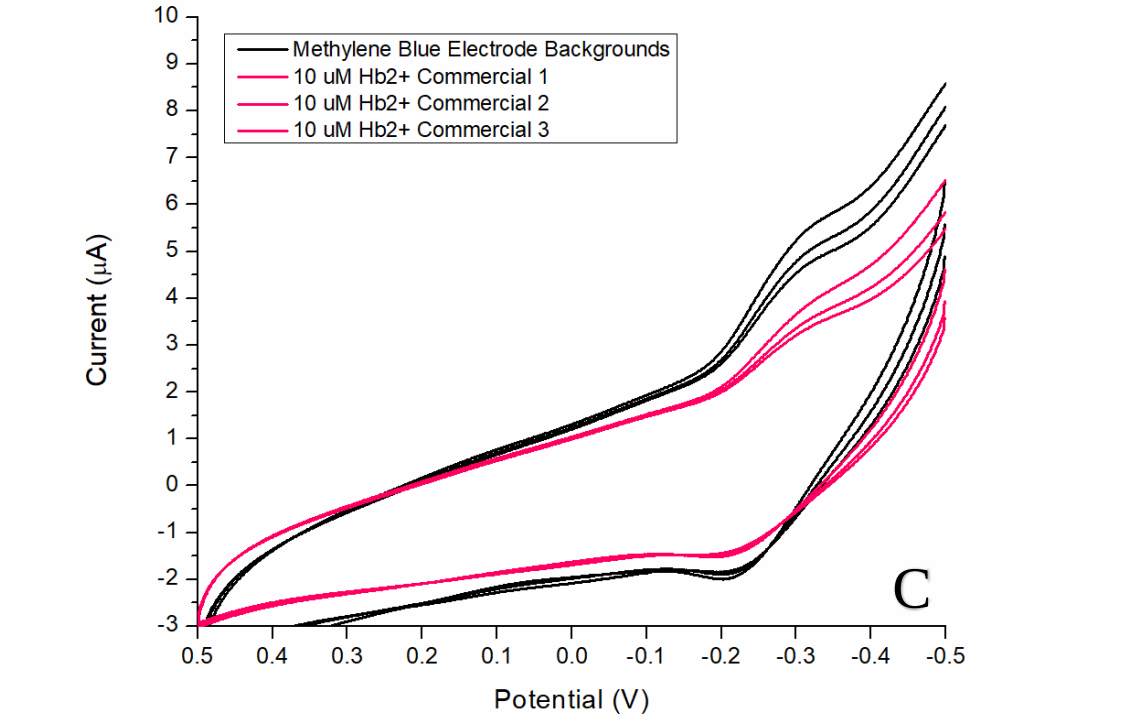
Methylene Blue Electrode Backgrounds
10 uM Hb2+ Commercial 1
10 uM Hb2+ Commercial 2
10 uM Hb2+ Commercial 3
Current (μA)
Potential (V)
C

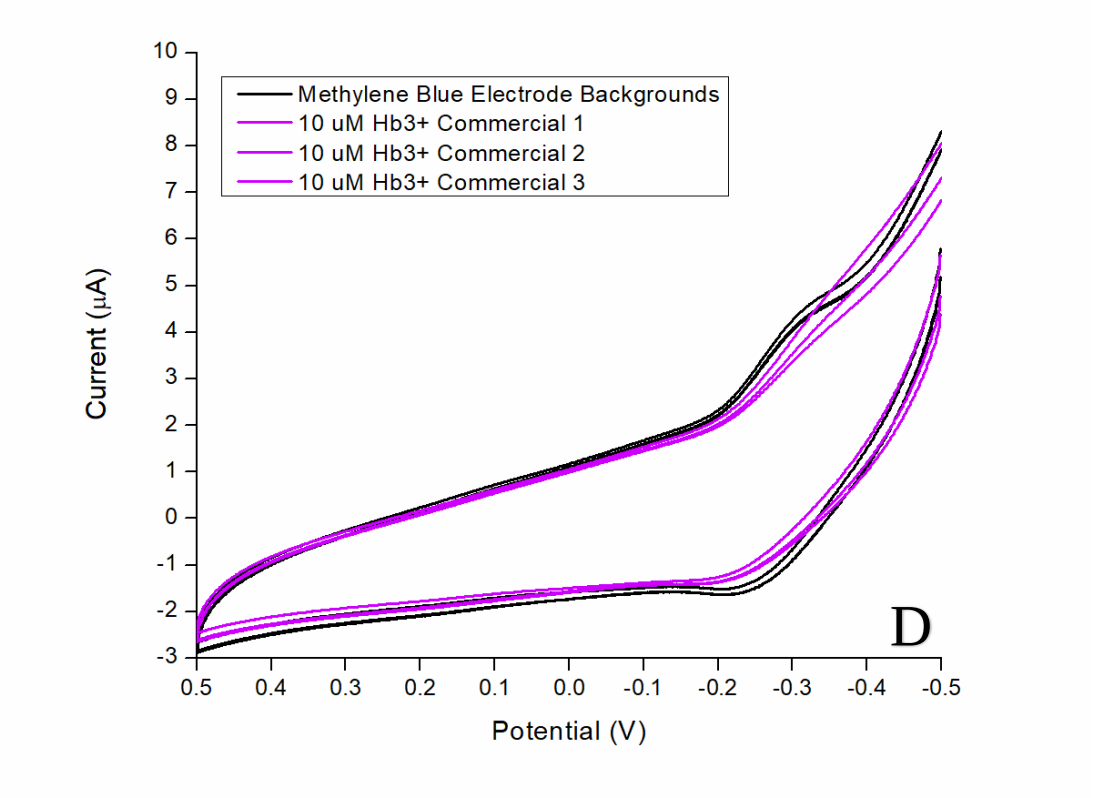

Figure 8.1. Freshly Isolated and Commercial Ferric and Ferrous Hemoglobin Cyclic Voltammograms. Planar glassy carbon electrode (vs. Ag/AgCl) with methylene blue film was created and run in triplicate for each sample. A) The freshly isolated ferrous (Hb^{2+}) hemoglobin adheres to the expected behavior for the enzyme, catalytically enhancing the methylene blue reaction and showing a current response above the methylene blue. B) Freshly isolated ferric (Hb^{3+}) hemoglobin appears to have suppressed the catalytic activity of the methylene blue, as shown by the current response within the methylene blue. C) and D) the commercial Ferrous and Ferric hemoglobin samples respectively show similar behavior to graph B, catalytically inhibiting the methylene blue.

In figure 8.1A, the hemoglobin acts as expected with the CV approximately following the methylene blue films during the oxidative half of the scan. By starting at -0.5 V vs. Ag/AgCl instead of the $E_{1/2}$, the return reductive half of the scan results in the hemoglobin deviating from the methylene blue CVs instead of forming peaks at the reductive peak potential, the hemoglobin flat lines instead. This indicates that the freshly isolated Hb^{2+} is assisting in the catalysis of the methylene blue redox, therefore increasing the current. In figure 8.1B, the freshly isolated Hb^{3+} shows a different outcome. The initial scan from +0.5 to -0.5 shows a current response lower than the methylene blue, meaning that it has somehow stopped this current response from occurring, instead of following the methylene blue CV or enhancing it (as it should if acting benign in solution or participating in catalysis). While not actively surpassing as previously, the reverse oxidation scan does not show the enhancement it should. Specifically, what is significant is that this is where the accumulation of the entire surface should lead to the flat-lining off of the peak, which does not occur.

The commercial samples show the inactivity and suppression described earlier, with the Hb^{2+} being the worst offender (figure 8.1C). The commercial Hb^{3+} does not seem to deviate from the methylene blue film. Curiously in the data, the Hb^{3+} samples seem to demonstrate the flat-lining during the initial reduction scan, with the curve of the oxidation half of the reaction being present (even if below the baseline of the methylene blue baseline).

The suppression within Figure 8.1B, C, and D ultimately suggest that the hemoglobin displaces the methylene blue from the surface and adsorbs in its place.

8.1.4. Conclusions & Future Outlooks

There are concerns with both the effectiveness of methylene blue as an effective sensing platform for hemoglobin and the use of commercial hemoglobin. Based upon the previous

literature as to how the methylene blue film works mechanistically, the most electro-catalytically active enzyme is the ferrous hemoglobin that has been freshly isolated and converted via new non-chemical methods by Afzal *et al.* Issues with replication caused these results to be challenging to achieve, and the need to have a different sensor film for each sample. Large scale use of this film for sensor development is inadvisable at this time.